FEB 3 1986
DATE ISSUED

ORNL
MASTER COPY

ORNL/TM-9741

ornl

OAK RIDGE
NATIONAL
LABORATORY

MARTIN MARIETTA

Oxidation/Corrosion of Metallic and Ceramic Materials in an Aluminum Remelt Furnace

J. I. Federer
P. J. Jones

OPERATED BY
MARTIN MARIETTA ENERGY SYSTEMS, INC.
FOR THE UNITED STATES
DEPARTMENT OF ENERGY

Printed in the United States of America. Available from
National Technical Information Service
U.S. Department of Commerce
5285 Port Royal Road, Springfield, Virginia 22161
NTIS price codes—Printed Copy: A05 Microfiche A01

This report was prepared as an account of work sponsored by an agency of the United States Government. Neither the United States Government nor any agency thereof, nor any of their employees, makes any warranty, express or implied, or assumes any legal liability or responsibility for the accuracy, completeness, or usefulness of any information, apparatus, product, or process disclosed, or represents that its use would not infringe privately owned rights. Reference herein to any specific commercial product, process, or service by trade name, trademark, manufacturer, or otherwise, does not necessarily constitute or imply its endorsement, recommendation, or favoring by the United States Government or any agency thereof. The views and opinions of authors expressed herein do not necessarily state or reflect those of the United States Government or any agency thereof.

ORNL/TM-9741

METALS AND CERAMICS DIVISION

OXIDATION/CORROSION OF METALLIC AND CERAMIC MATERIALS IN AN ALUMINUM REMELT FURNACE

J. I. Federer and P. J. Jones

NOTICE: This document contains information of a preliminary nature. It is subject to revision or correction and therefore does not represent a final report.

Date Published: December 1985

Prepared for the
Assistant Secretary for Conservation and
Renewable Energy, Office of Industrial
Programs, Waste Energy Recovery Program

Prepared by the
OAK RIDGE NATIONAL LABORATORY
Oak Ridge, Tennessee 37831
operated by
MARTIN MARIETTA ENERGY SYSTEMS, INC.
for the
U.S. DEPARTMENT OF ENERGY
under Contract No. DE-AC05-84OR21400

CONTENTS

ABSTRACT 1
INTRODUCTION 2
MATERIALS 4
RESULTS 6
CHARACTERIZATION OF COATED ALLOYS 6
AIR OXIDATION TESTS 10
ALUMINUM REMELT FURNACE TESTS 30
Flue Gas Corrosion/Fouling Deposits 30
Uncoated and Coated Alloys 33
Ceramic Materials 50
SUMMARY 56
CONCLUSIONS 58
ACKNOWLEDGMENTS 59
REFERENCES 59

TABLES

Table 1. Nominal composition of materials 5

Table 2. Weight changes of uncoated and coated alloys oxidized at 1000°C 16

Table 3. Weight changes of uncoated alloys oxidized at 1100°C 18

Table 4. Composition of flue gas corrosion/fouling deposits 31

Table 5. Crystalline phases in flue gas corrosion/fouling deposits . 32

Table 6. Materials and exposure periods in aluminum remelt furnace flue gases 33

Table 7. Corrosion rates of materials exposed to aluminum remelt furnace flue gases at 1000 to 1100°C 49

FIGURES

Fig. 1. Fluidized bed waste heat recovery system 3

Fig. 2. Aluminum-coated alloys supplied by Alon and TCC 7

Fig. 3. Aluminum-coated alloys showing relative hardnesses of coatings, diffusion zones, and substrates 8

Fig. 4. Backscattered electron image of type 316/Al (Alon) 9

Fig. 5. Characteristic X-ray displays of Inconel 625/Al (TCC) . . . 11

Fig. 6. Silica-coated alloys provided by Aremco and CRC 12

Fig. 7. Characteristic X-ray displays of type 316/SiO_2 (Aremco) . . 13

Fig. 8. Characteristic X-ray displays of type 316/SiO_2 (CRC) 14

Fig. 9. Uncoated alloys after 1000 h at 1000°C in air 16

Fig. 10. Uncoated alloys after 1136 h at 1100°C in air 19

Fig. 11. Characteristic X-ray displays of type 310 after oxidation at 1100°C for 1136 h in air 20

Fig. 12. Electron microprobe analysis of the oxide layer and near surface region of type 310 21

Fig. 13. Characteristic x-ray displays of Hastelloy X after oxidation at 1100°C for 1136 h in air 23

Fig. 14. Backscattered electron images of microconstituents in Hastelloy X after oxidation at 1100°C for 1136 h in air . . 24

Fig. 15. Electron microprobe analysis of Hastelloy X after oxidation at 1100°C for 1136 h in air 25

Fig. 16. Coated alloys heat treated at 1000°C for 500 h in air . . . 27

Fig. 17. Coated alloys heat treated at 1000°C for 1000 h in air . . . 28

Fig. 18. Microstructures of coated alloys heat treated at 1000°C for 1000 h in air 29

Fig. 19. Uncoated Inconel 625 exposed to flue gases 34

Fig. 20. Characteristic X-ray displays of corroded Inconel 625 . . . 36

Fig. 21. Inconel 625/Al (TCC) after exposure to flue gases for 2250 h 37

Fig. 22. Inconel 625/Al (TCC) after exposure to flue gases for 2250 h 38

Fig. 23. Inconel 625/Al (TCC) after exposure to flue gases 39

Fig. 24. Characteristic X-ray displays of Inconel 625/Al (TCC) after exposure to flue gases 41

Fig. 25. Characteristic X-ray displays of Inconel 625/Al (TCC) after exposure to flue gases 42

Fig. 26. Inconel 625/SiO_2 (Aremco) after exposure to flue gases for 3110 h 43

Fig. 27. Inconel 601/Al (Alon) after exposure to flue gases for 1200 h 44

Fig. 28. Haynes 188/Al (Alon) after exposure to flue gases for 1200 h 45

Fig. 29. Haynes 188/Al (Alon) after exposure to flue gases for 4030 h 46

Fig. 30. Uncoated Alloy 214 after exposure to flue gases 47

Fig. 31. Sintered-α and NC-430 SiC ceramics after exposure to flue gases for 4300 h 52

Fig. 32. SiC ceramics after exposure to flue gases for 4300 h 53

Fig. 33. Oxide ceramics after exposure to flue gases for 4300 h . . . 55

OXIDATION/CORROSION OF METALLIC AND CERAMIC MATERIALS IN AN ALUMINUM REMELT FURNACE*

J. I. Federer and P. J. Jones

ABSTRACT

Both metallic alloys and ceramic materials are candidates for the distributor plate and other components of fluidized bed waste heat recovery (FBWHR) systems. Eleven Fe-, Ni-, and Co-base alloys were exposed to air at elevated temperatures in laboratory furnaces and to flue gases in an aluminum remelt furnace to assess their resistance to oxidation and corrosion. Four SiC ceramics and two oxide ceramics were also tested in the aluminum remelt furnace. Some alloys were coated with aluminum or SiO_2 by commercial processes in an effort to enhance their oxidation and corrosion resistance.

Uncoated alloys tested at 1000 and 1100°C in air had mostly small specific weight changes, but all had surface scales, subsurface porosity (or oxidation), and some exhibited intergranular attack. The aluminum coatings generally protected the substrates against oxidation, but SiO_2 coatings detached and were not effective.

Uncoated Inconel 625 exposed to aluminum remelt furnace flue gases at 1000 to 1100°C exhibited extensive intergranular attack, which proceeded at a projected rate of 2.6 mm/y. Corrosion in this environment exceeded that observed in air oxidation tests. In some cases aluminum-coated Inconel 625 corroded more slowly (1.2 mm/y) in the aluminum remelt furnace than uncoated material; however, aluminum coatings were not always protective to this or other alloys. Silica coatings, as in air oxidation tests, detached and did not provide any protection against attack. The corrosion rate of SiC ceramics in the aluminum remelt furnace was significantly less (0.5 mm/y) than that of alloys. High purity alumina, which was least affected of all materials tested, exhibited no measurable corrosion after an exposure of 4300 h.

Based on corrosion behavior, metallic alloys are only marginally suitable for components to be exposed to high temperature aluminum remelt furnace flue gases in FBWHR systems. Use of these materials would require continuous monitoring of corrosion. Silicon carbide ceramics and oxide ceramics, which exhibit better oxidation and corrosion resistance than the alloys, are still prime candidates for these applications.

---

*Research sponsored by the Waste Energy Recovery Program, Office of Industrial Programs, U.S. Department of Energy, under contract DE-AC05-84OR21400 with Martin Marietta Energy Systems, Inc.

Potential disadvantages with the ceramic materials compared to alloys include more complex fabricability, plus lower toughness and resistance to thermal shock.

INTRODUCTION

In recent years the Department of Energy has sponsored several high-temperature waste-heat recovery projects in cooperation with industrial participants.[1,2,3] The goal of these projects is to develop systems for preheating combustion air by recovering waste heat from high-temperature, corrosive/fouling flue gases. The system that was being developed by Thermo Electron Corporation (TECO) is a Fluidized Bed Waste Heat Recovery System (FBWHRS).[3] This system consists of two fluidized beds as shown in Fig. 1. Flue gases from an industrial furnace fluidize and heat alumina particles in the upper bed. The particles are recirculated between the upper and lower beds, as shown, resulting in heating of combustion air. The preheated air causes a higher flame temperature for a given amount of fuel, thereby resulting in fuel savings.

An industrial aluminum remelt furnace was selected by TECO as the host site for testing and development of the FBWHRS. Aluminum remelting represents significant industrial energy use and, therefore, a significant potential for energy savings. Furthermore, furnace practice results in high-temperature particle-laden flue gases, which might be corrosive to many materials of construction. Successful development of an FBWHRS for aluminum remelt furnaces, therefore, would enhance their acceptability for other types of industrial furnaces.

Materials of construction for the FBWHRS are required to have acceptable resistance to corrosion and oxidation by high-temperature flue gases. The distributor plate in the upper bed (Fig. 1) is one of the critical components in the system because it is in direct contact with flue gases at temperatures up to 1100°C. Silicon carbide and oxide ceramics have been considered for the distributor plate; however, ceramic plates of large areas containing numerous small holes are not readily available. In addition, oxide ceramics, such as alumina and mullite,

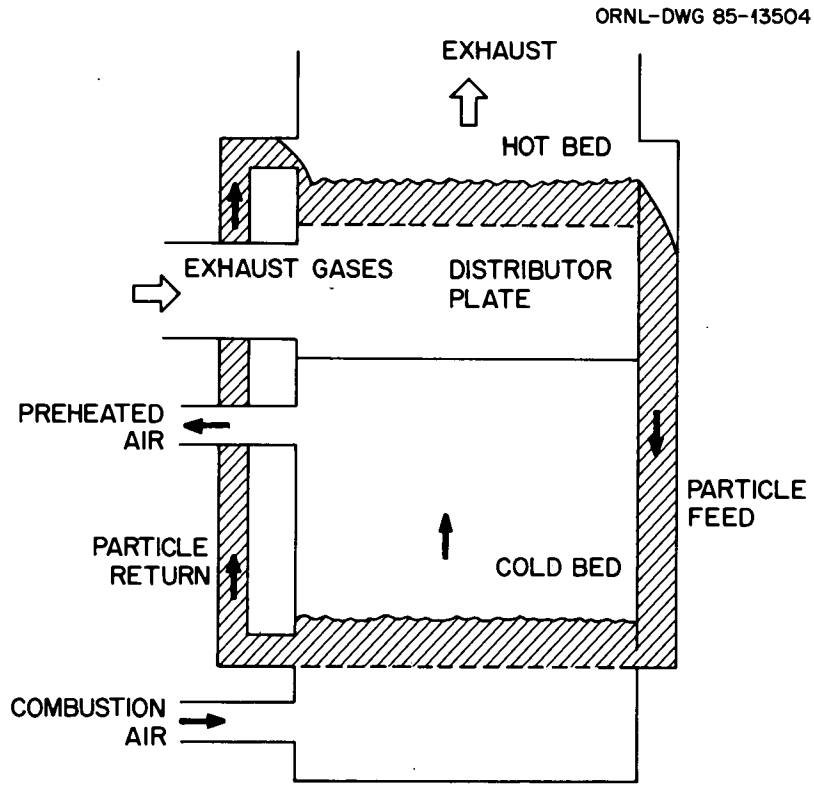

Fig. 1. Fluidized bed waste heat recovery system. *Source:* W. E. Cole, R. de Saro, and C. Joshi, *Fluidized-Bed Waste-Heat Recovery System Development, Semiannual Report, February 1–July 31, 1983,* DOE/ID/12302-4. Modified for this report.

might not have satisfactory thermal-shock resistance for this application. Consequently, metallic alloys were selected as interim materials for critical components of the FBWHRS until ceramic components are available. Because of potential corrosion problems, the metallic alloys were subjected to exposure tests to characterize their corrosion/oxidation behavior. These exposure tests and analyses of specimens were conducted cooperatively by TECO and ORNL using the host aluminum remelt furnace for exposure to flue gases and laboratory furnaces for tests in air.

Several metallic alloys, both coated and uncoated, and several ceramic materials were included in the exposure tests. Subsequently the exposed specimens were subjected to conventional examinations including measurement of changes in weights and dimensions; microstructural examination; and chemical, X-ray diffraction, and electron microprobe analyses.

MATERIALS

Candidate materials of construction including metallic alloys, coatings, and ceramic materials are shown in Table 1. The metallic alloys were selected to represent Fe-, Ni-, and Co-base compositions with a range of oxidation and corrosion resistances and high-temperature strengths. These alloys are commercially available as sheet, plate, and other forms. Distributor plates for the FBWHRS could be made by drilling or otherwise forming the required holes in sheet or plate stock of the alloys. The ceramic materials represent several commercially available compositions. Although not as readily fabricable into distributor plates, these materials were included in some exposure tests for comparison with the alloys. Three types of SiC ceramics were tested: sintered-α SiC, siliconized or reaction sintered SiC (NC-430 and Refel), and Si_3N_4-bonded SiC (Refrax 20). The two oxides included in the test, alumina and mullite, are highly refractory ceramic materials.

Substrates of several alloys in the form of plain or perforated sheet were coated with aluminum by commercial manufacturers (Table 1). Interdiffusion of aluminum and the substrates, either during coating or a

Table 1. Nominal composition of materials

Materials	Composition, wt %																	Manufacturers
	Al	Co	Cr	Cu	Fe	La	Mo	Nb	Ni	Si	Ti	W	Y	Al_2O_3	SiC	Si_3N_4	SiO_2	
Metallic alloys																		
Type 316			17		bal.		3		12									
Type 310			25		bal.				21									
Type 446			25		bal.													
Incoloy 800	0.4		22		39.5				33									Huntington Alloys
Inconel 601	1.5		23	1	bal.				60									Huntington Alloys
Inconel 625	0.4	1	22		5		10	3.7[a]	58		0.4							Huntington Alloys
Hastelloy X		1.5	22		19		10		bal.			0.5						Cabot Corp.
Hastelloy N	0.5[b]	0.2	27	0.4	5		17		bal.			0.5						Cabot Corp.
Alloy 214	5		16		4				bal.				0.4					Cabot Corp.
Haynes 25		bal.	20		3				10			15						Cabot Corp.
Haynes 188		bal.	22		3	0.1			22			15						Cabot Corp.
Coatings																		
Silica [SiO_2(Aremco)]																	>99	Aremco Products, Inc.
Aluminum [Al(Alon)]	>99																	Alon Processing, Inc.
Silica [SiO_2(CRC)]																	>99	Ceramic Refractory Corp.
Aluminum [Al(TCC)]	>99																	Turbine Components Corp.
Ceramic materials																		
Sintered-α SiC															>99			Carborundum Co.
NC-430 SiC										10.6					88.5			Norton Co.
Refel SiC										10					90			Pure Carbon Co.
Refrax 20 SiC														2.7	73	21	3	Carborundum Co.
AD-998 Alumina														99.8			<0.1	Coors Porcelain Co.
Mullite														70			28	Coors Porcelain Co.

[a] Nb+Ta.

[b] Al+Ti.

subsequent heat treatment, promotes bonding by formation of alloys and/or intermetallic compounds between aluminum and the principal constituents of the alloys. Exposure of the coated alloys to an oxidizing environment results in formation of aluminum oxide or mixed oxides at the surface in contact with the environment. The oxide layer minimizes access of oxygen and other chemical species to the alloys and, if intact, can provide significant protection against oxidation and corrosion of the substrates. Substrates of several alloys were also coated with SiO_2 by two manufacturers (Table 1). Unlike aluminum coatings, very little interdiffusion of SiO_2 and the substrates occurred. Protection of the substrate requires that the SiO_2 coatings be sufficiently thick and dense to minimize passage of oxygen or other corrodents to the substrate. Selection of SiO_2 as a coating in this work was based on the high melting point, the fact that it is a stable oxide under expected recuperator conditions, and available coating technology. As will be shown, the SiO_2 coatings provided less protection than aluminum coatings when exposed either to air or flue gases at elevated temperatures.

RESULTS

CHARACTERIZATION OF COATED ALLOYS

The microstructures of typical aluminum-coated alloys are shown in Fig. 2. The coatings were metallic in appearance, cracked in some areas, and often had porosity at the coating-substrate interface. A diffusion zone is evident in the type 316 alloy. Figures 2(*g*) and (*h*) show that the coating thicknesses on an outer surface and on the inner surface of a 2.5-mm-diam hole were approximately equal. Figure 3 shows the relative hardnesses of coatings, diffusion zones, and substrates. The relatively high hardness of the coatings suggests the presence of intermetallic compounds; however, this was not confirmed by analysis.

Coatings were also characterized prior to exposure by electron microprobe analyses. Figure 4 is a backscattered electron (BSE) picture of type 316/Al (Alon) showing locations of elemental analyses. The

ORNL PHOTO 4238-85

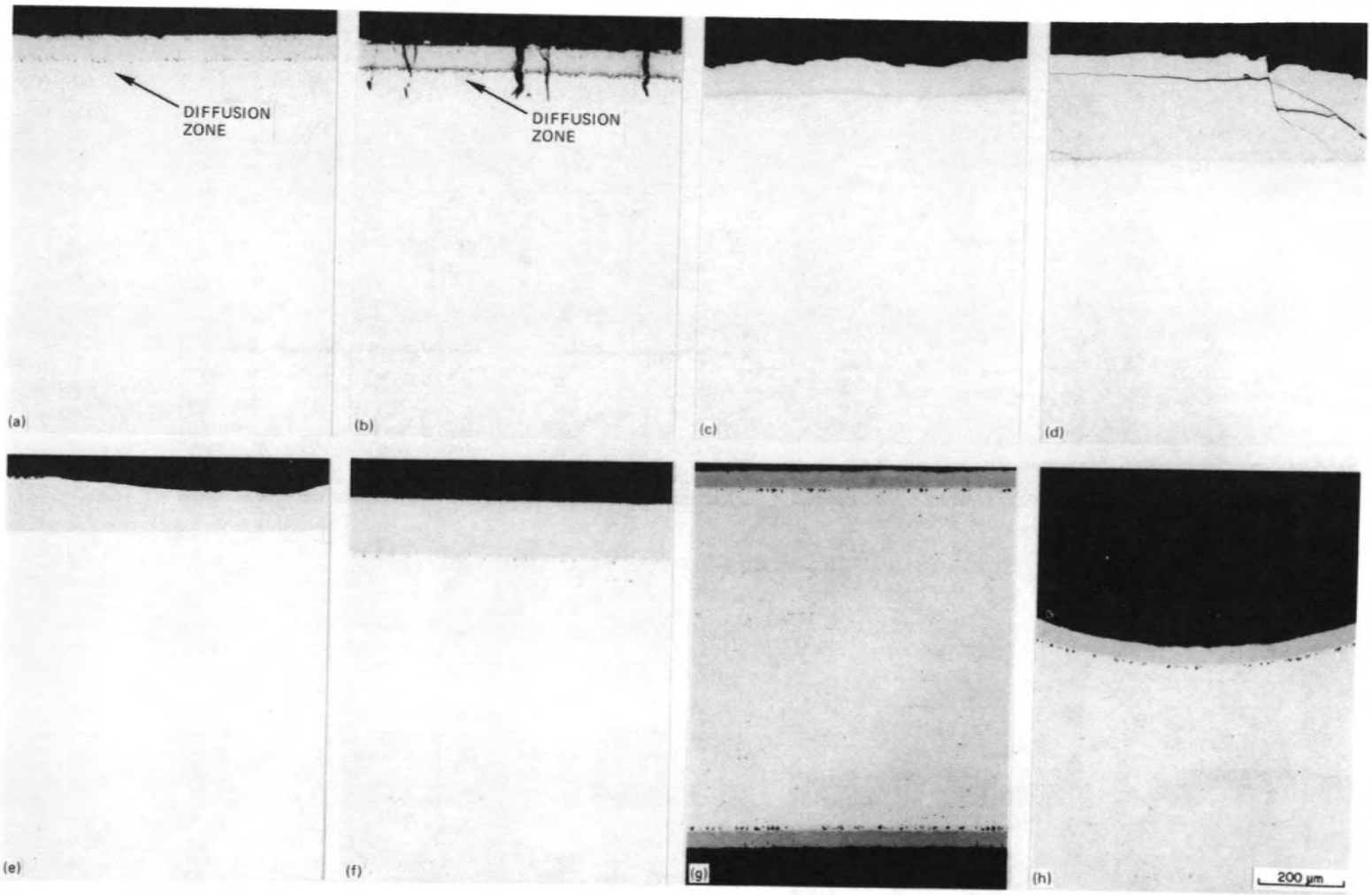

Fig. 2. Aluminum-coated alloys supplied by Alon and TCC. (*a*) and (*b*) Type 316/Al (Alon), (*c*) and (*d*) Inconel 601/Al (Alon), (*e*) Haynes 188/Al (Alon), (*f*) Inconel 625/Al (Alon), (*g*) and (*h*) Inconel 625/Al (TCC). As polished.

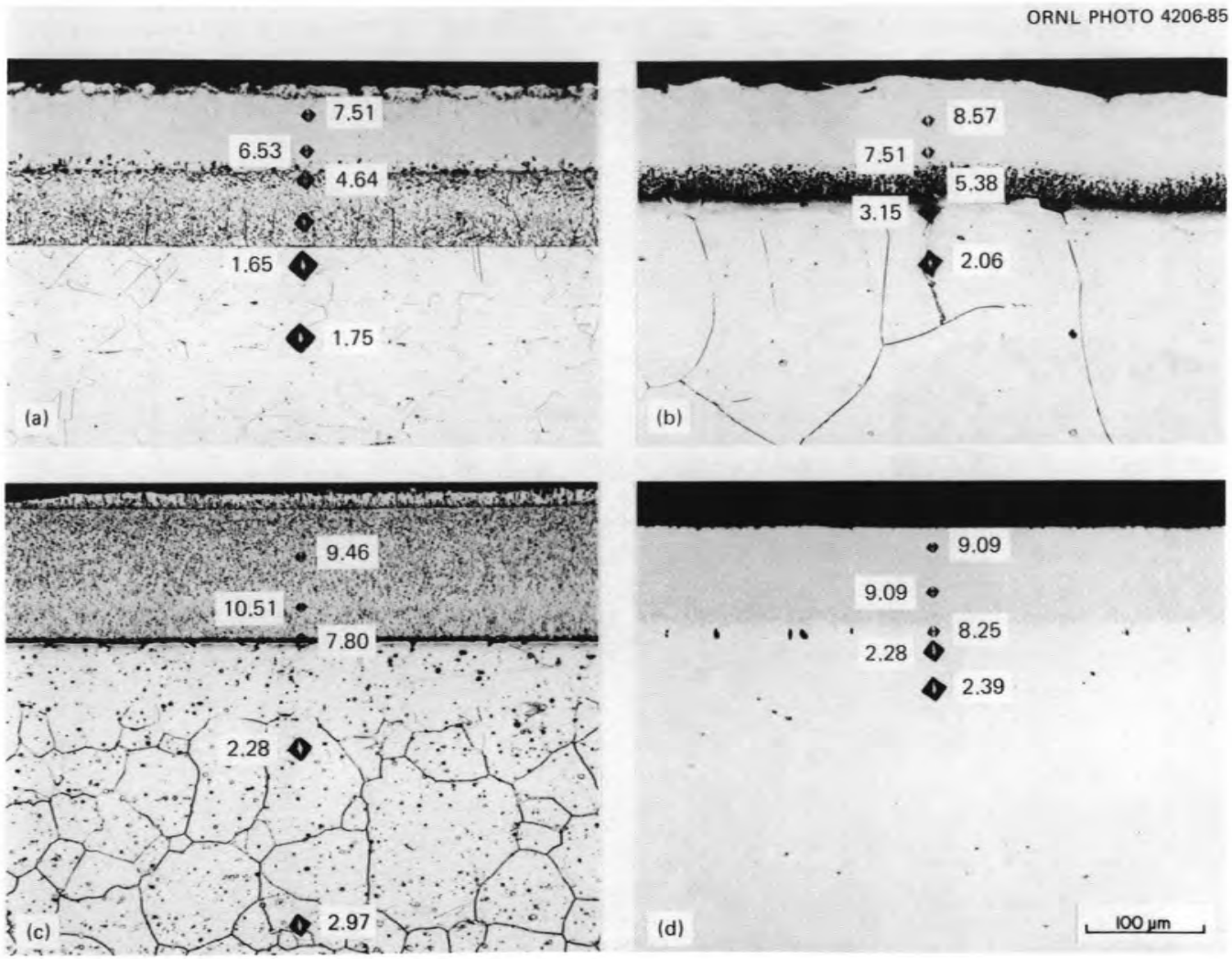

Fig. 3. Aluminum-coated alloys showing relative hardnesses of coatings, diffusion zones, and substrates. Hardness unit is GPa. All except (*d*) were etched.

ORNL PHOTO 4207-85

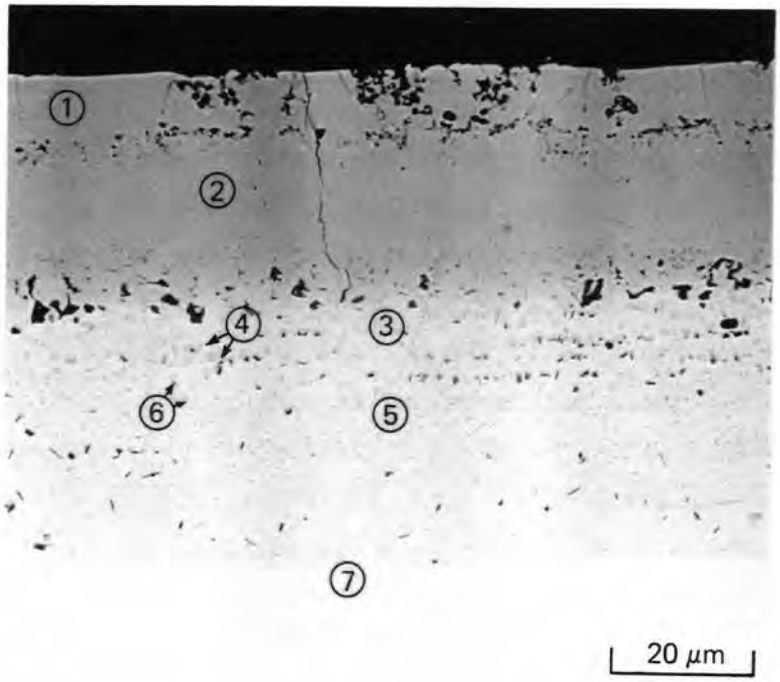

AREA	REFERENCE	COMPOSITION (wt %) Fe	Ni	Cr	Mo	Al
COATING	1	51.3	3.8	8.3	0.5	30.8
COATING	2	49.0	7.3	7.9	0.9	31.1
MATRIX OF DIFFUSION ZONE	3	58.4	6.2	20.4	2.9	9.5
PARTICLE IN DIFFUSION ZONE	4	32.4	35.7	8.1	1.0	20.8
MATRIX OF DIFFUSION ZONE	5	65.0	4.2	19.8	2.5	4.0
PARTICLE IN DIFFUSION ZONE	6	56.0	13.6	17.1	1.9	9.2
SUBSTRATE	7	67.2	10.4	17.4	2.0	<0.1

Fig. 4. Backscattered electron image of type 316/Al (Alon).

results of the analyses showed that considerable interdiffusion of Al and the substrate had occurred. The outer layer contained mostly Fe and Al, as shown by analysis of Areas 1 and 2. The diffusion zone consisted of small gray particles in a light gray matrix. The particles and matrix were analyzed at two locations relative to the outer layer. At both locations the particles contained higher concentrations of Al and Ni than the adjacent matrix (Areas 3, 4, 5, and 6). The substrate (Area 7), which contained very little Al, exhibited approximately the concentrations of Fe, Cr, Ni, and Mo shown by the nominal composition of type 316 in Table 1.

Figure 5 shows a BSE image and characteristic X-ray displays for Inconel 625/Al (TCC). The coating, diffusion zone, and substrate are clearly shown in the BSE picture. The X-ray elemental displays revealed high concentrations of Al and Ni in the outer layer, Cr in the diffusion zone and in particles in the outer layer, and Ni and Cr in the substrate. Electron microprobe analyses of different areas confirmed the elemental distributions indicated by X-ray displays.

The results show that interdiffusion between coatings and alloy substrates has occurred. This interdiffusion generates adherence between coating and substrate. The coatings appear to be well bonded to the substrates in Fig. 2; however, the bond strength and durability are probably related to the relative coefficients of thermal expansion of coating, diffusion zone, and substrate and to the severity and number of thermal cycles.

Silica-coated alloys provided by Aremco and Ceramic Refractory Corp. are shown in Fig. 6. Some coatings were dark and porous, as indicated by intrusion of mounting compound during preparation for metallographic examination, while others appeared to be relatively dense. Hardness indentations in the coatings were so distorted that measurements could not be made, while those in the substrate indicated higher hardnesses near the coating-substrate interface. Characteristic X-ray displays in Figs. 7 and 8 showed that the coatings consisted mostly of Si and O.

AIR OXIDATION TESTS

Uncoated and coated alloys were exposed to air at 1000 and 1100°C for 1000 and 1136 h, respectively, to aid in interpreting corrosion behavior

ORNL PHOTO 4208-85

AREA	LOCATION	COMPOSITION, wt % Fe	Ni	Cr	Mo	Al
COATING	1	2.1	55.9	4.0	0.3	33.6
PARTICLE IN COATING	2	2.2	34.3	20.4	11.1	25.5
DIFFUSION ZONE	3	4.9	46.2	26.6	12.5	3.8
DIFFUSION ZONE	4	6.1	34.6	27.9	20.1	1.1
SUBSTRATE	5	4.2	58.2	23.0	9.1	0.4
SUBSTRATE	6	3.9	60.0	22.2	9.1	0.3

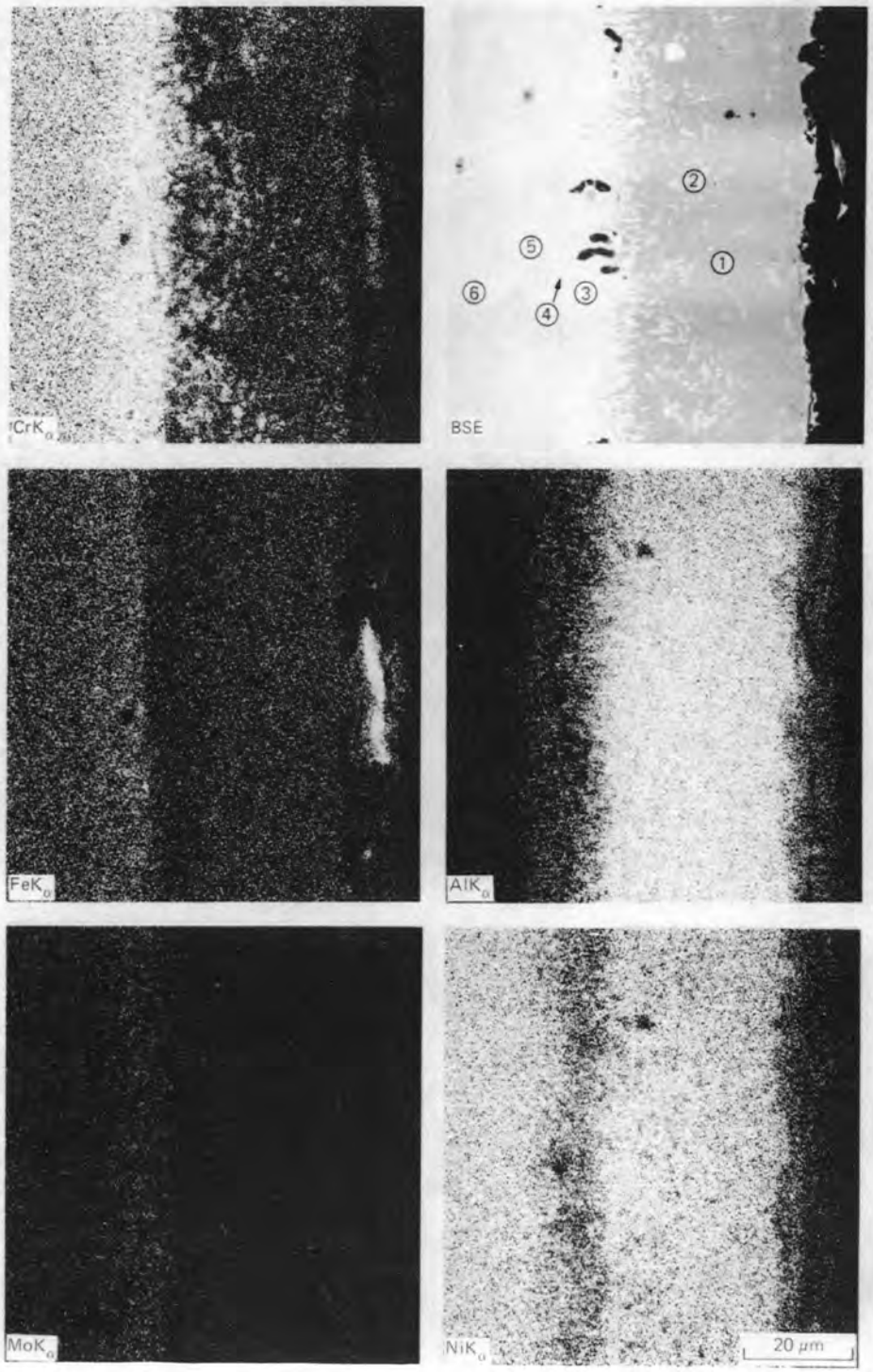

Fig. 5. Characteristic X-ray displays of Inconel 625/Al (TCC).

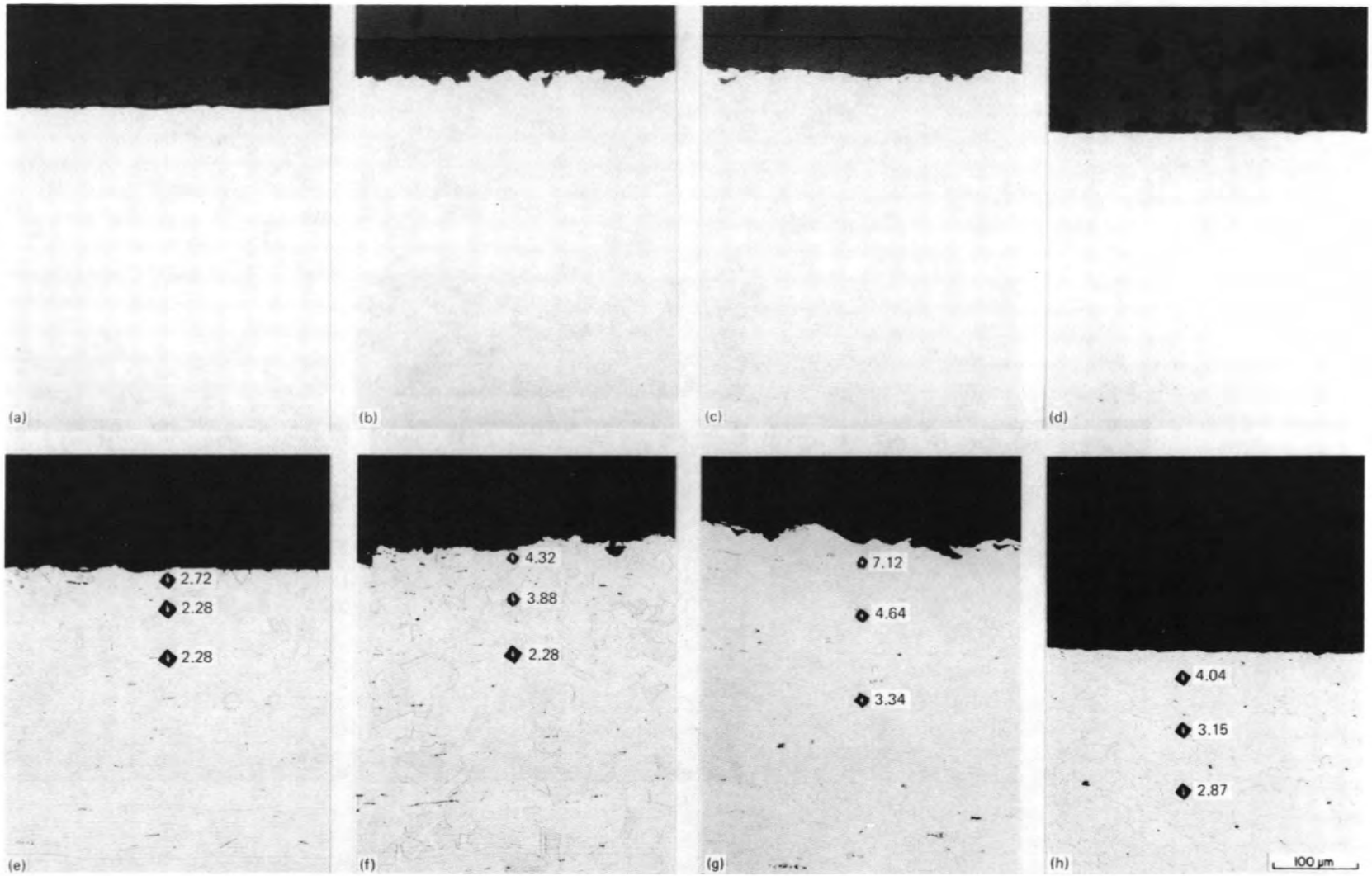

Fig. 6. Silica-coated alloys provided by Aremco and CRC. (*a*) and (*e*) Type 316/SiO_2 (Aremco), (*b*) and (*f*) Type 316/SiO_2 (CRC), (*c*) and (*g*) Inconel 625/SiO_2 (Aremco), (*d*) and (*h*) Inconel 625/SiO_2 (CRC). Unit of hardness is GPa. Top row as polished. Bottom row etched.

ORNL PHOTO 4254-85

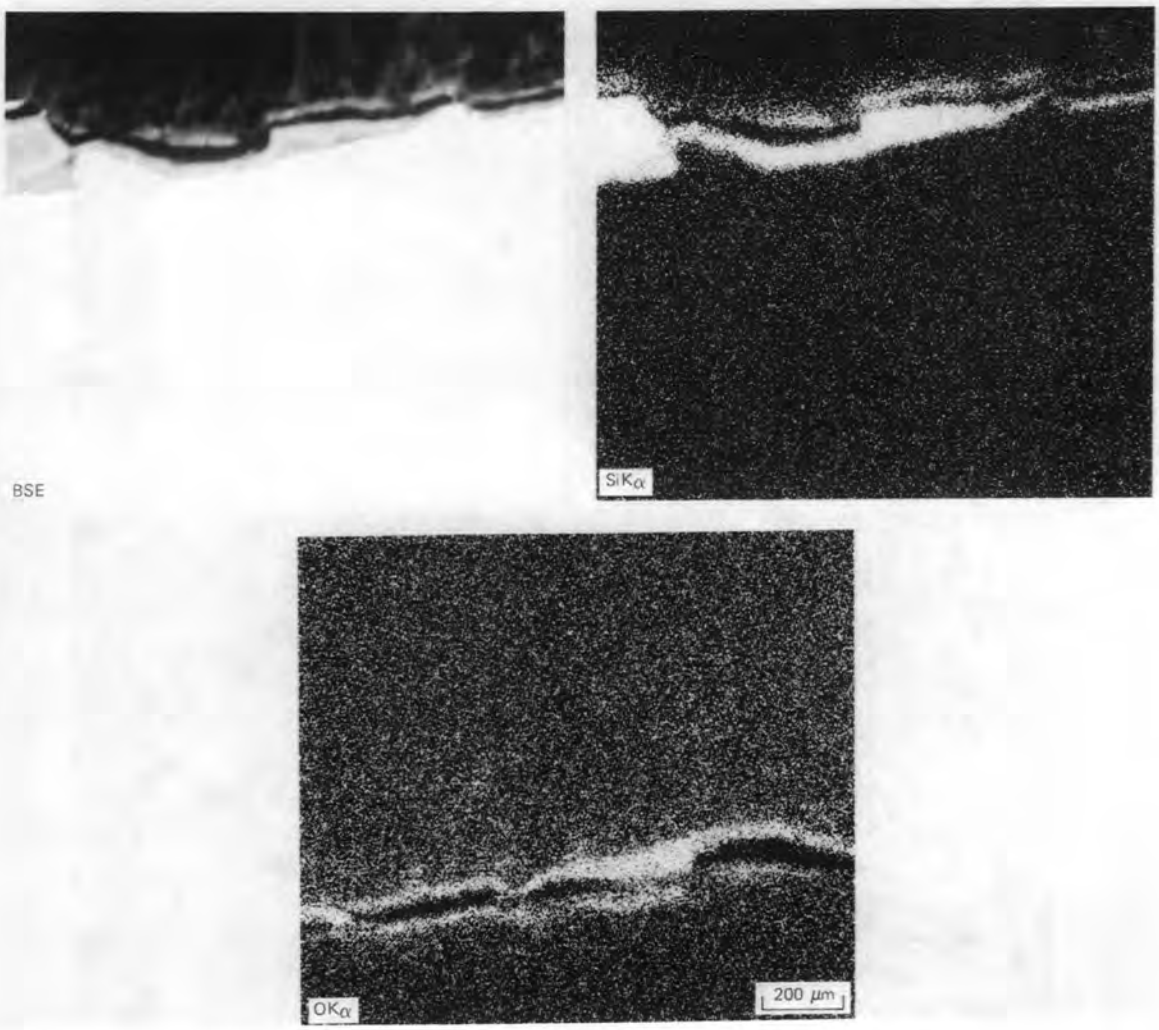

Fig. 7. Characteristic X-ray displays of type 316/SiO_2 (Aremco).

ORNL PHOTO 4255-85

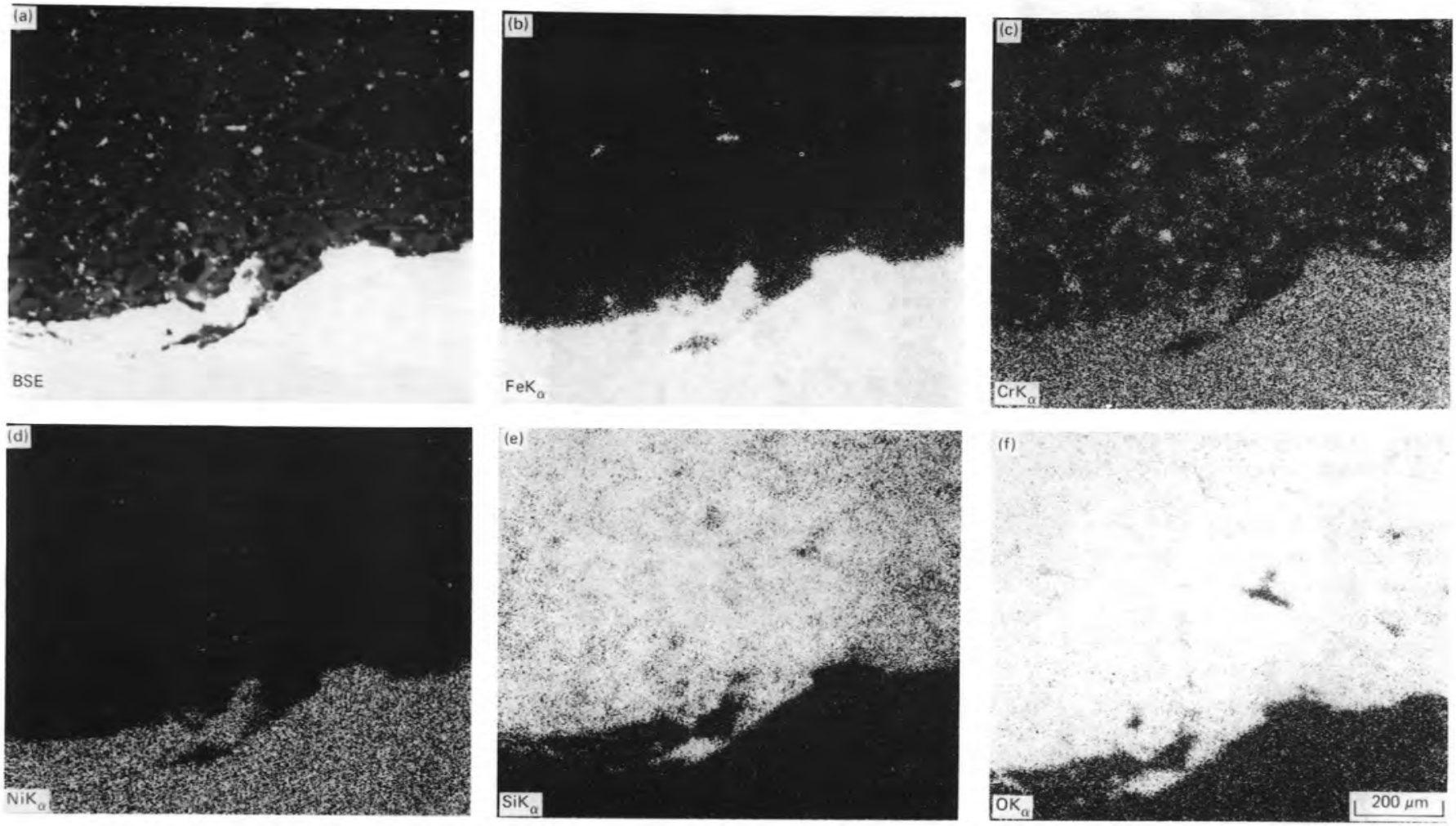

Fig. 8. Characteristic X-ray displays of type 316/SiO_2 (CRC).

of alloys exposed to flue gases in the host furnace. The effects of oxidation were determined by weight and microstructural changes. Rectangular samples of various thicknesses were supported on their edges in slots in a refractory brick for these tests. The samples were held at temperature in still air without thermal cycling except for an intermediate examination after approximately 500 h. Loosely adhering scale was removed with a soft bristle brush before obtaining intermediate and final weights.

Weight changes that occurred during the test at 1000°C are shown in Table 2. None of the uncoated alloys, except type 316, had significant weight changes after 504 or 1000 h. For example, a change of 0.2 $ng/cm^2 \cdot s$ for type 310 could have been caused by uniform oxidation to a depth of about 0.6 μm, and a change of −0.1 $ng/cm^2 \cdot s$ could have been caused by uniform loss of material to a depth of about 0.4 μm. The type 316 specimen oxidized extensively during the 504-h exposure, which resulted in swelling and spalling of the oxide.

The weight changes for coated alloys were also small except for the type 316 specimens. Coatings of Al and SiO_2 provided some protection to type 316 during the initial 504-h exposure, but not during the subsequent exposure when extensive oxidation and spalling occurred. Unfortunately, the specimens were not coated on the four edges. Undoubtedly oxidation began at the edges and eventually disrupted the coatings. Although this test unfairly portrayed the protective ability of the coatings on type 316, the catastrophic result of a defective coating on this material is clearly implied.

Micrographs of the oxidized surfaces of the uncoated alloys after exposure to air at 1000°C are shown in Fig. 9. Thin oxide layers on the surfaces, grain-boundary oxidation, and pore formation characterize these alloys except Alloy 214, which exhibited relatively little oxidation, mostly in the form of stringers extending about 0.05 mm into the specimen. Weight changes alone, therefore, do not adequately describe the effect of high temperature oxidation on these materials. The weight changes might not have occurred only at the surfaces. Substrate pore formation might have been caused either by vaporization of one or more constituents or by diffusion of one or more elements into the oxide layer.

Table 2. Weight changes of uncoated and coated alloys oxidized at 1000°C

Alloy	Coating	Initial weight (g)	Initial area (cm^2)	Weight change $ng/cm^2 \cdot s$ after	
				504 h	1000 h
Type 316	None	23.61	64.02	*a*	
Type 310	None	34.95	82.89	0.2	<–0.1
Type 446	None	16.29	51.79	0.7	0.4
Incoloy 800	None	21.63	58.91	–0.6	–0.5
Inconel 601	None	146.47	121.36	0.2	0.1
Inconel 625	None	17.92	73.75	0.5	0.3
Hastelloy X	None	5.15	62.66	0.4	0.2
Hastelloy N	None	126.67	113.94	–1.3	–1.2
Alloy 214	None	18.67	51.17	0.1	0.1
Haynes 25	None	46.07	70.18	–0.6	–0.2
Haynes 188	None	16.92	61.16	0.2	0.1
Type 316	SiO_2 (Aremco)[b]	4.73	27.40	36.0	
Type 316	Al (Alon)[c]	6.12	33.92	–0.8	
Type 316	SiO_2 (CRC)[d]	9.70	53.38	–6.9	
Inconel 601	Al (Alon)	11.91	30.95	0	0.1
Inconel 625	SiO_2 (Aremco)	11.71	30.02	0.6	0.6
Inconel 625	Al (Alon)	11.16	28.79	0.4	0.6
Inconel 625	SiO_2 (CRC)	25.17	61.56	2.0	1.2
Haynes 188	Al (Alon)	11.44	34.29	–0.2	0

[a]Extensive oxidation and spalling occurred.

[b]Aremco Products, Inc., Ossining, N.Y.

[c]Alon Processing Inc. Tarentum, Penn.

[d]Ceramic Refractory Corp., Transfer, Penn.

Table 3 shows the weight changes that occurred in uncoated alloys during oxidation in air at 1100°C. Incoloy 800, Hastelloy N, and Haynes 25 were affected more than the other alloys. The weight change of –21.5 $ng/cm^2 \cdot s$ for Incoloy 800 could have been caused by uniform loss of material to a depth of about 0.11 mm. Figure 10 shows micrographs of eight alloys after the exposure at 1100°C. Grain-boundary attack and pore formation were more severe at 1100°C than at 1000°C (Fig. 9).

ORNL PHOTO 4239-85

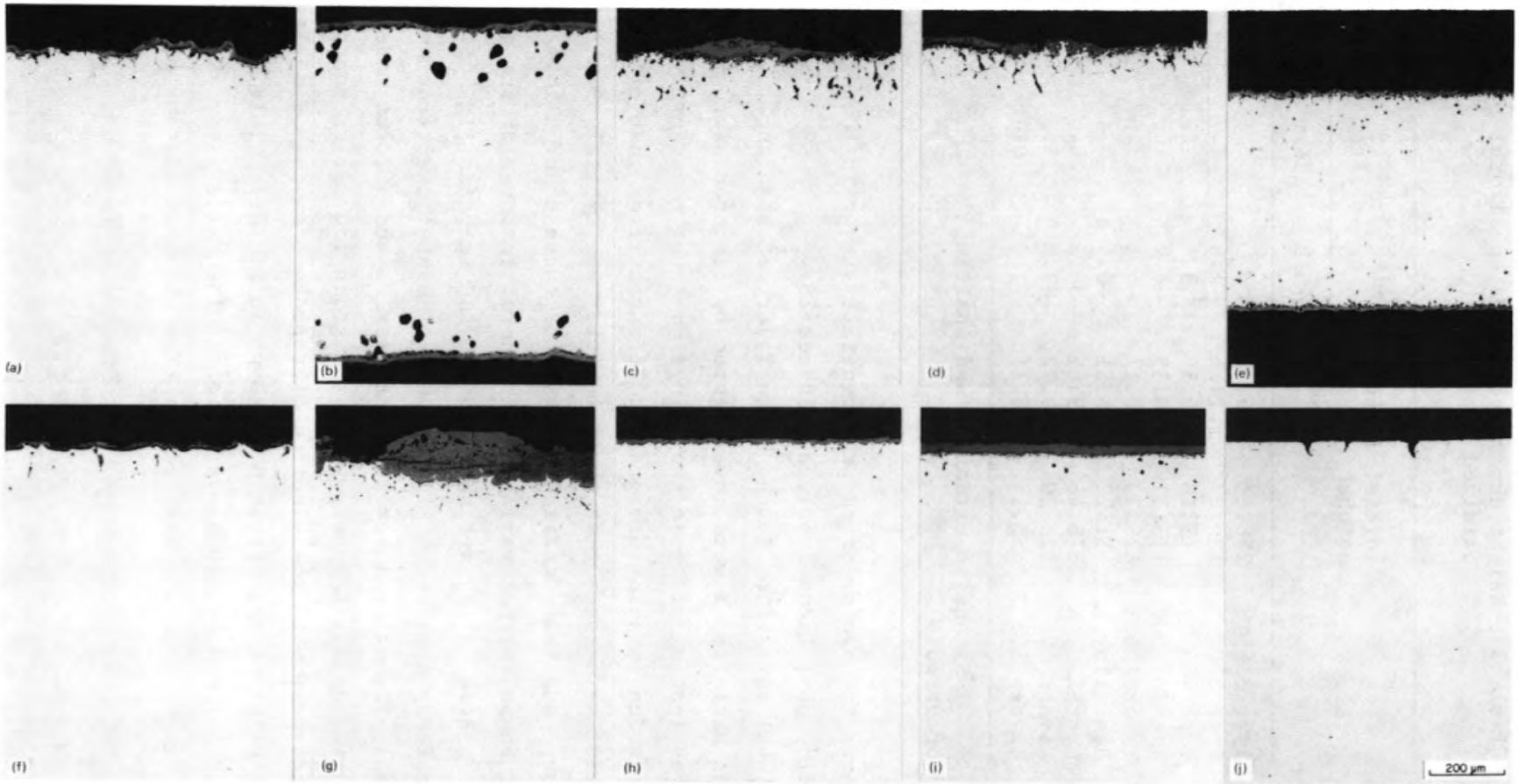

Fig. 9. Uncoated alloys after 1000 h at 1000°C in air. (*a*) Type 310, (*b*) Type 446, (*c*) Incoloy 800, (*d*) Inconel 601, (*e*) Hastelloy X, (*f*) Hastelloy N, (*g*) Haynes 25, (*h*) Haynes 188, (*i*) Inconel 625, (*j*) Alloy 214. As polished.

Table 3. Weight changes of uncoated alloys oxidized at 1100°C

Alloy	Initial weight (g)	Initial area (cm^2)	Weight change $ng/cm^2 \cdot s$ after	
			475 h	1136 h
Type 316	258.86	306.47	[a]	
Type 310	130.87	111.75	−1.6	−2.7
Type 446	19.18	55.50	3.4	2.8
Incoloy 800	115.31	110.33	−4.2	−21.5
Inconel 601	423.35	109.17	−5.1	−3.5
Hastelloy X	11.72	55.61	−0.5	−0.4
Hastelloy N	376.46	109.81	−86.5	−128.0
Haynes 25	226.20	119.72	−83.0	−125.5
Haynes 188	55.14	75.75	1.0	0.4

[a]Extensive oxidation and spalling occurred.

Oxidation appears to have occurred preferentially at grain boundaries of type 310, Incoloy 800, Inconel 601, and Haynes 25.

Compositional variations in the oxide layer and adjacent region of type 310 and Hastelloy X were investigated by electron microprobe analysis. Investigation of these two alloys does not necessarily mean that their oxidation behavior was greatly different from that of the other alloys. Instead, we suspect that their behavior was typical of alloys within the group, and that detailed analyses of these other alloys would reveal similar compositional variations. General features of the surface region of the oxidized alloy are shown in the BSE image in Fig. 11. Characteristic X-ray spectra in Fig. 11 show elemental distributions in the same region. The oxide layer contains less Fe and Ni, but more Cr, O, and Si than the adjacent metal, while the grain boundaries contain more O and Si. A traverse with the electron microprobe from the oxide layer towards the interior of the specimen is shown in Fig. 12. This analysis reveals substantial compositional variations. The oxide layer is chromium-rich relative to the base metal. The chromium content of the

ORNL PHOTO 4252-85

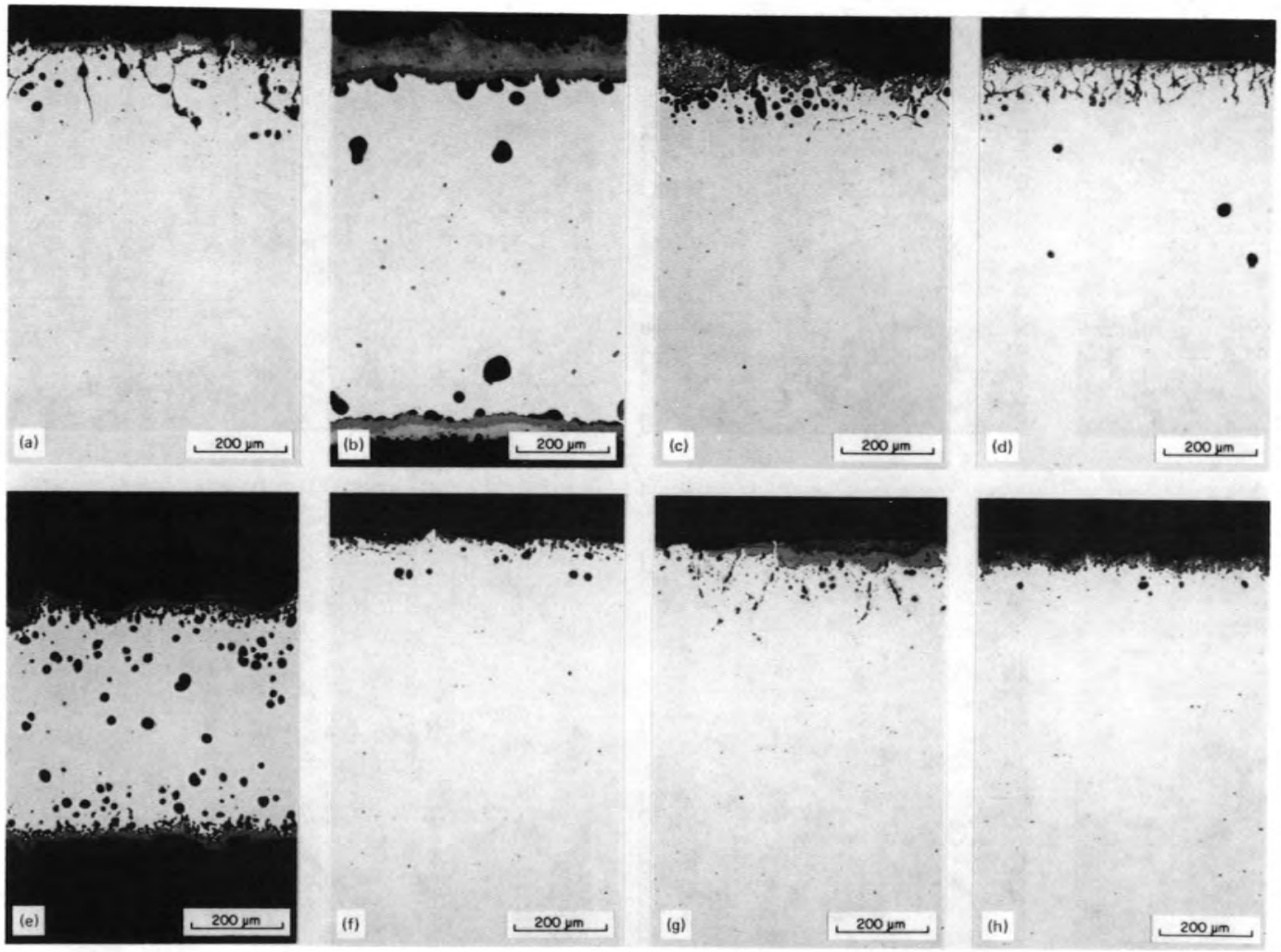

Fig. 10. Uncoated alloys after 1136 h at 1100°C in air. (*a*) Type 310, (*b*) Type 446, (*c*) Incoloy 800, (*d*) Inconel 601, (*e*) Hastelloy X, (*f*) Hastelloy N, (*g*) Haynes 25, (h) Haynes 188. As polished.

ORNL PHOTO 4251-85

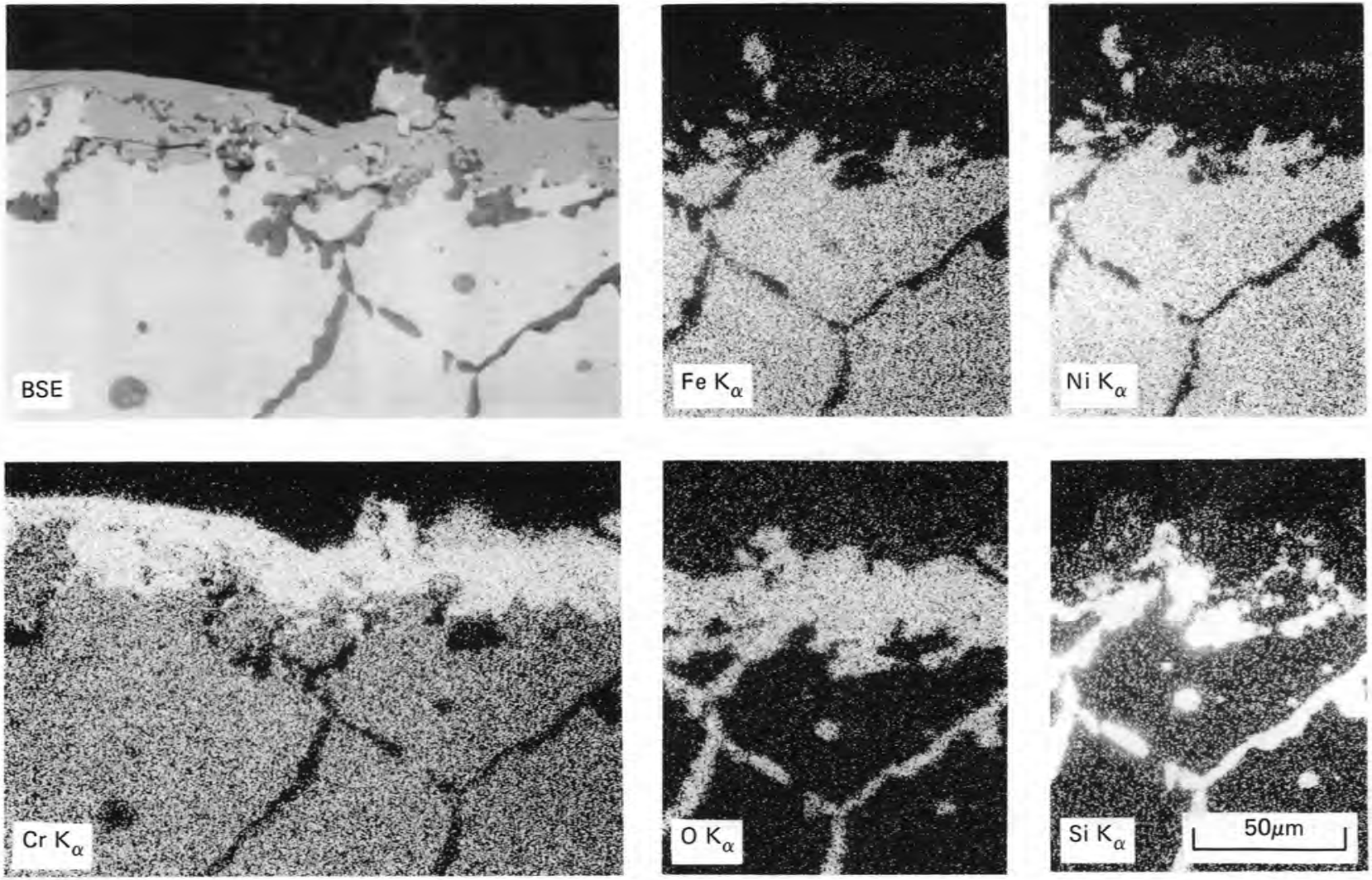

Fig. 11. Characteristic X-ray displays of type 310 after oxidation at 1100°C for 1136 h in air.

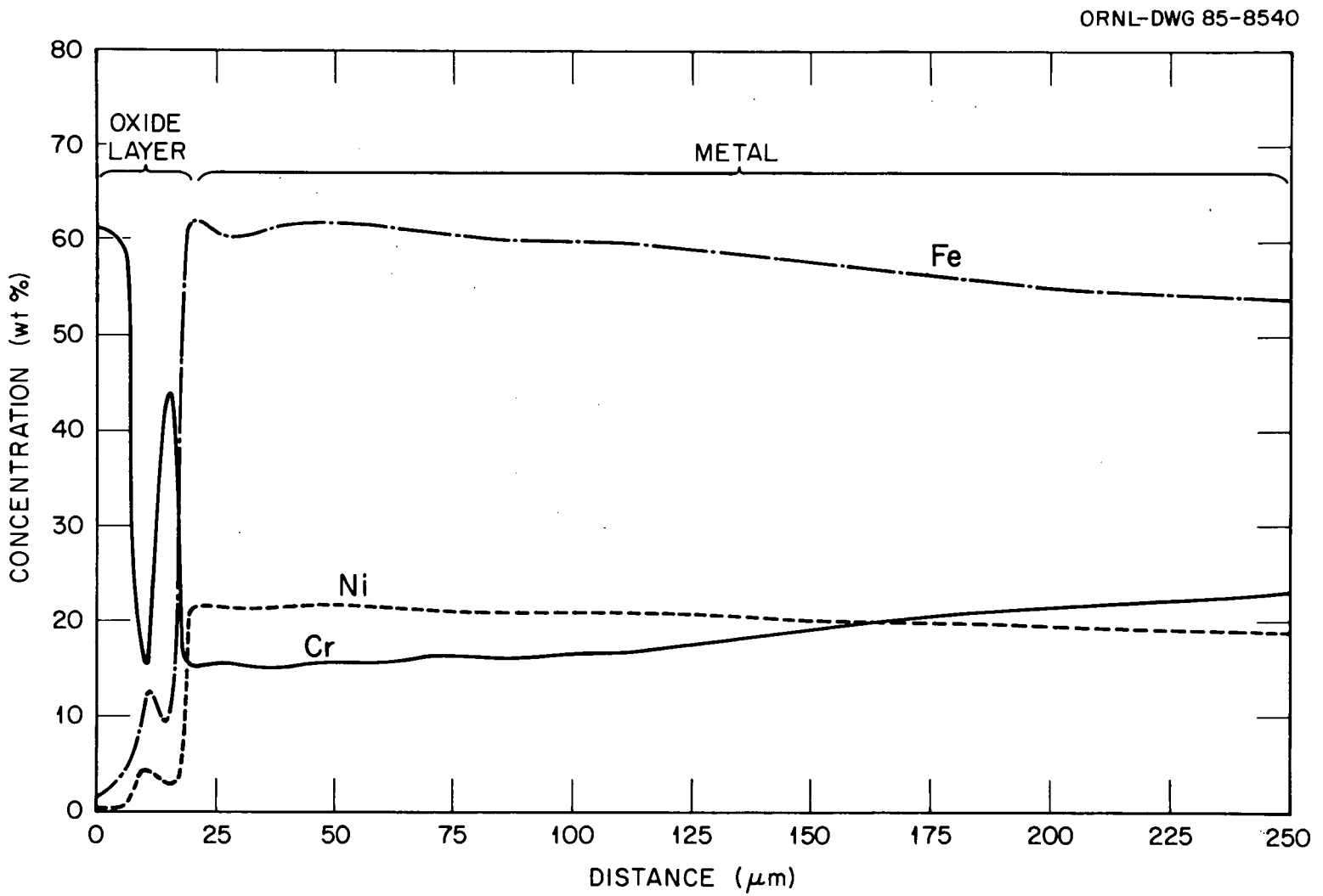

Fig. 12. Electron microprobe analysis of the oxide layer and near surface region of type 310.

metal near the oxide layer is about 15%, but approaches the original Cr content of the alloy (~25%) with increasing distance into the alloy.

These results show that the oxidation mechanism involves preferential diffusion of Cr and Si to the surface and oxidation to Cr_2O_3 and SiO_2. Since these oxides are thermodynamically stable relative to the metals in an oxidizing atmosphere at 1100°C, their formation is the driving force for diffusion to the surface. The depletion of Cr in the near surface region results in a composition that has less resistance to oxidation than the original alloy. The compositional change associated with different diffusion rates of the principal constituents in the alloy (Fe, Cr, and Ni) probably also results in the formation of apparent pores, which are actually isolated regions of Cr_2O_3 and SiO_2.

Substantial compositional variations were also shown in the Hastelloy X specimen by electron microprobe analysis. Characteristic X-ray spectra in Fig. 13 reveal that the oxide coating contains mostly Cr and O. Backscattered electron images (Fig. 14) show small black and white microconstituents in a region near the surface. The results of electron microprobe traverses through these regions are shown in Fig. 15. Traverses through the oxide layer and adjacent region showed that Cr, the major metallic element in the oxide layer, decreased in the interfacial region, finally obtaining a constant value in the alloy. Nickel, Fe, and Mo, which were present in very small concentrations in the oxide, increased in the interfacial region to constant levels in the alloy. The interfacial region is a mixture of alloy and oxide as evidenced by the undulating traces for the four elements. A traverse through the Mo-containing white particles revealed steep gradients for Fe, Cr, Ni, and Mo at the interface between alloy and particle. Similarly, the black region was shown to contain less Fe, Cr, Ni, and Mo, but more Si, than the adjacent alloy.

Other investigators have observed similar results for several alloys exposed to air at elevated temperatures. Lai et al.[4] held type 310, Hastelloy X and Inconel 600 at 1150°C for up to 430 h in air. Each alloy had an oxide scale, grain-boundary attack, and subsurface pore (or oxide) formation. Alloy 214, however, exhibited practically no attack after 1000 h at 1150°C in air. The same investigators conducted short-time

ORNL PHOTO 4250-85

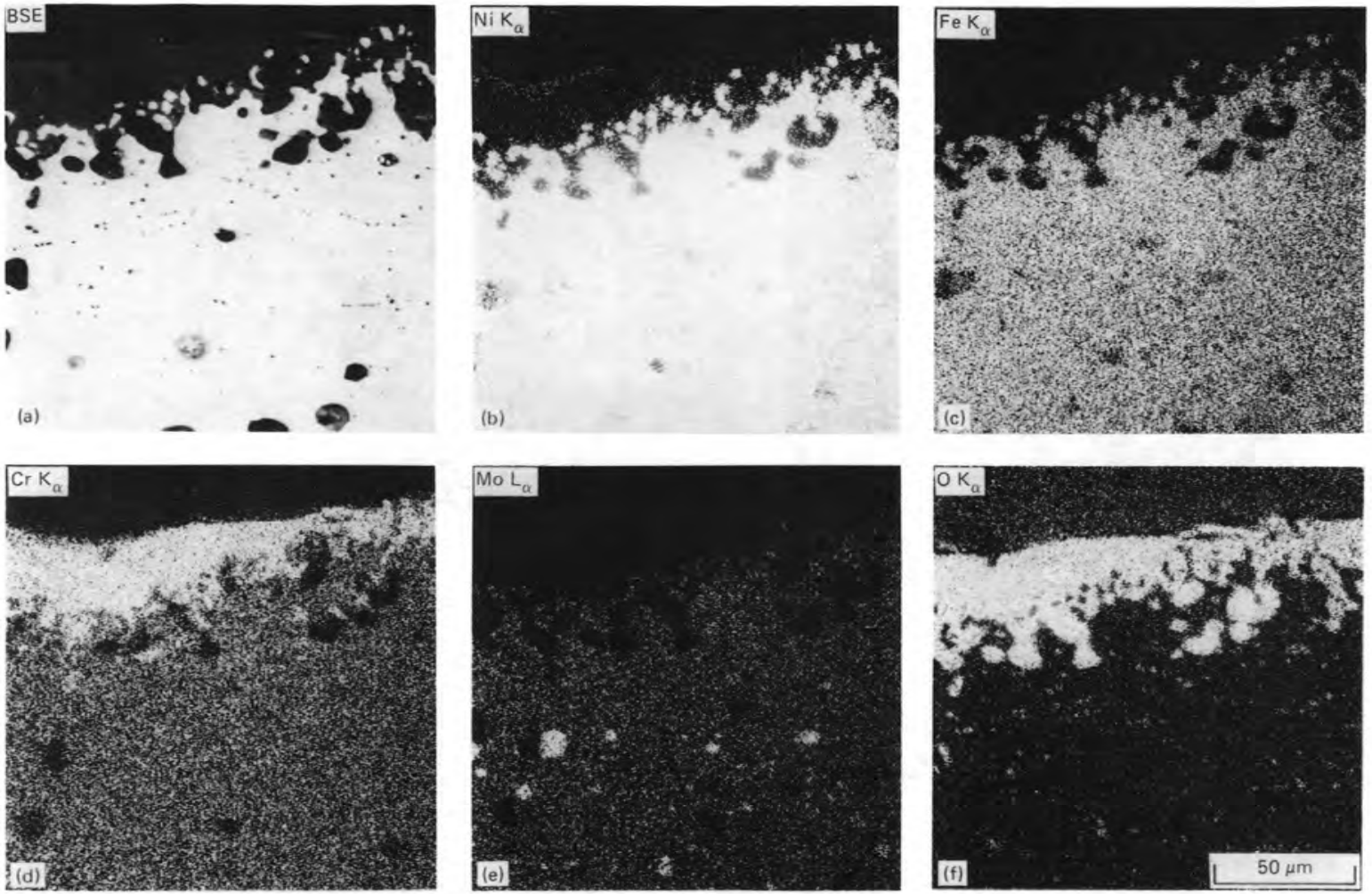

Fig. 13. Characteristic X-ray displays of Hastelloy X after oxidation at 1100°C for 1136 h in air.

ORNL PHOTO 4209-85

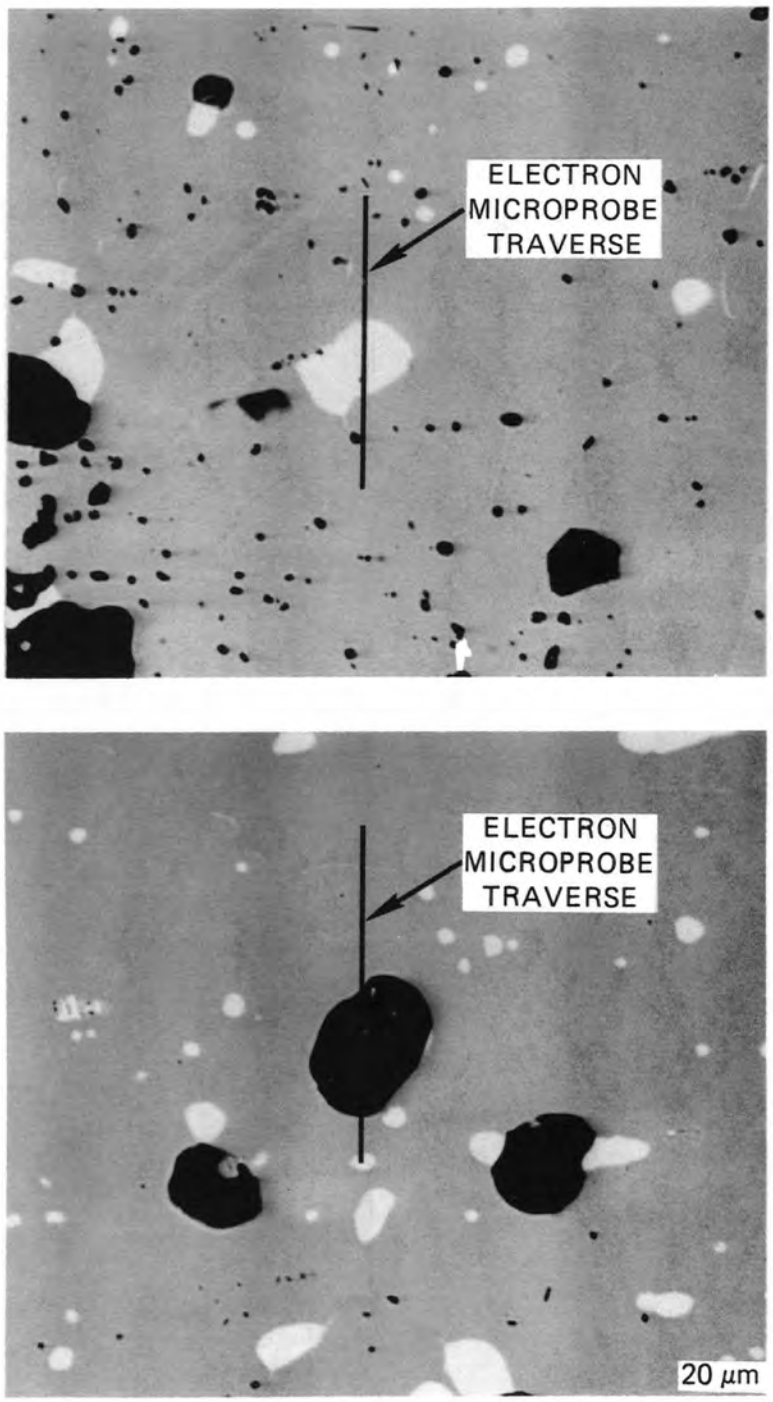

Fig. 14. Backscattered electron images of microconstituents in Hastelloy X after oxidation at 1100°C for 1136 h in air.

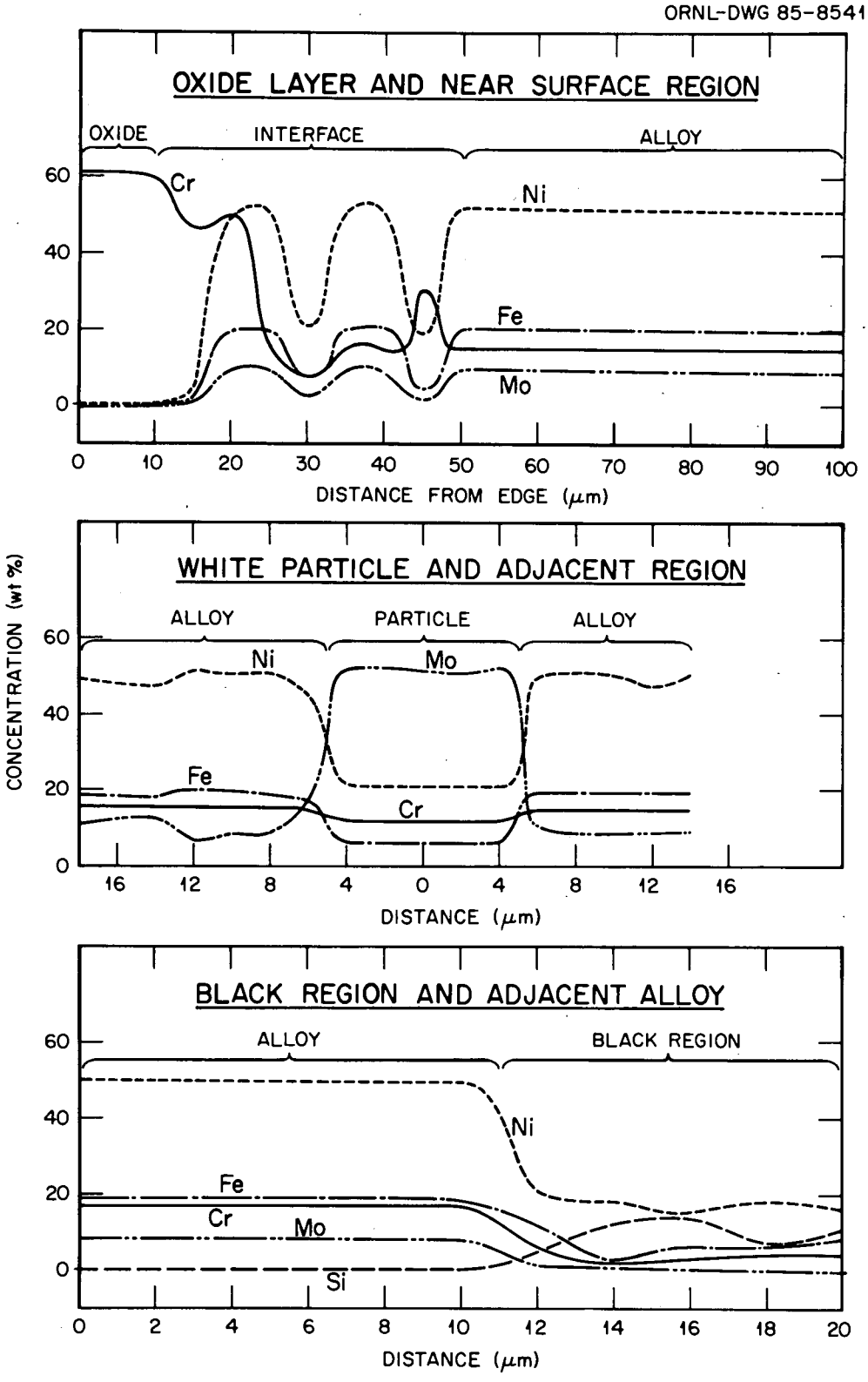

Fig. 15. Electron microprobe analysis of Hastelloy X after oxidation at 1100°C for 1136 h in air.

tests in oxidizing and reducing atmospheres containing Cl_2. A test of only 8 h at 900°C in an oxidizing atmosphere containing Cl_2 produced considerable scale formation, grain boundary attack, and subsurface pore formation in type 310, Incoloy 800 H, Inconel 600, Inconel 625, and Hastelloy S, while Alloy 214 had practically no attack except for occasional surface pits. All alloys were attacked in a similar test using a reducing atmosphere, but Alloy 214 seemed to be attacked least of all. Rao et al.[5] tested type 310, Incoloy 800 H, Inconel 601, and Alloy 214 at 1095°C for 1008 h. Each alloy, except Alloy 214, developed a surface scale and subsurface pore (or oxide) formation. Again, Alloy 214 was practically unattacked.

As previously mentioned both Al- and SiO_2-coated type 316 specimens were severely damaged as a result of oxidation. Figure 16 shows coated specimens of type 316 and Inconel 625 after 500 h at 1000°C in air. The type 316 specimens exhibited spalling, swelling, and cracking, while Inconel 625 exhibited only defoliation of the coating in some holes. After 1000 h at 1000°C in air the type 316 specimens showed substantially more degradation, as shown in Fig. 17. The other specimens showed relatively little damage; however, microstructural evidence of degradation of some materials is shown in Fig. 18. The SiO_2 coatings on Inconel 625 (Aremco and CRC) were mostly missing from the substrates as shown in Figs. 18(*a*) and (*c*), and the Al coating (Alon) on Inconel 625 partially degraded [Fig. 18(*b*)]. The Inconel 601/Al (Alon) specimen, shown in Fig. 18(*d*), exhibited a diffusion zone, which was not present in the as-coated material [Figs. 2(*c*) and (*d*)]. Some minor degradation, probably oxidation, is evident on the outer surface. The Haynes 188/Al (Alon) specimen exhibits similar minor degradation on the outer surface and also a crack in the interfacial region [Fig. 18(*e*)]. Reference to Table 2 shows that the three coated Inconel 625 specimens had larger weight changes (gains) than the relatively unaffected Inconel 601/Al (Alon) and Haynes 188/Al (Alon). Pore formation and/or subsurface oxides also occurred in most of the alloys. In the case of Inconel 625/SiO_2 (Aremco) and Inconel 625/SiO_2 (CRC) the pores are near the unprotected surfaces, as was previously shown for several uncoated alloys in Fig. 9. Pores in Inconel 625/Al (Alon) and Haynes 188/Al (Alon) occurred both in the interfacial region and at greater depth.

ORNL PHOTO 4211-85

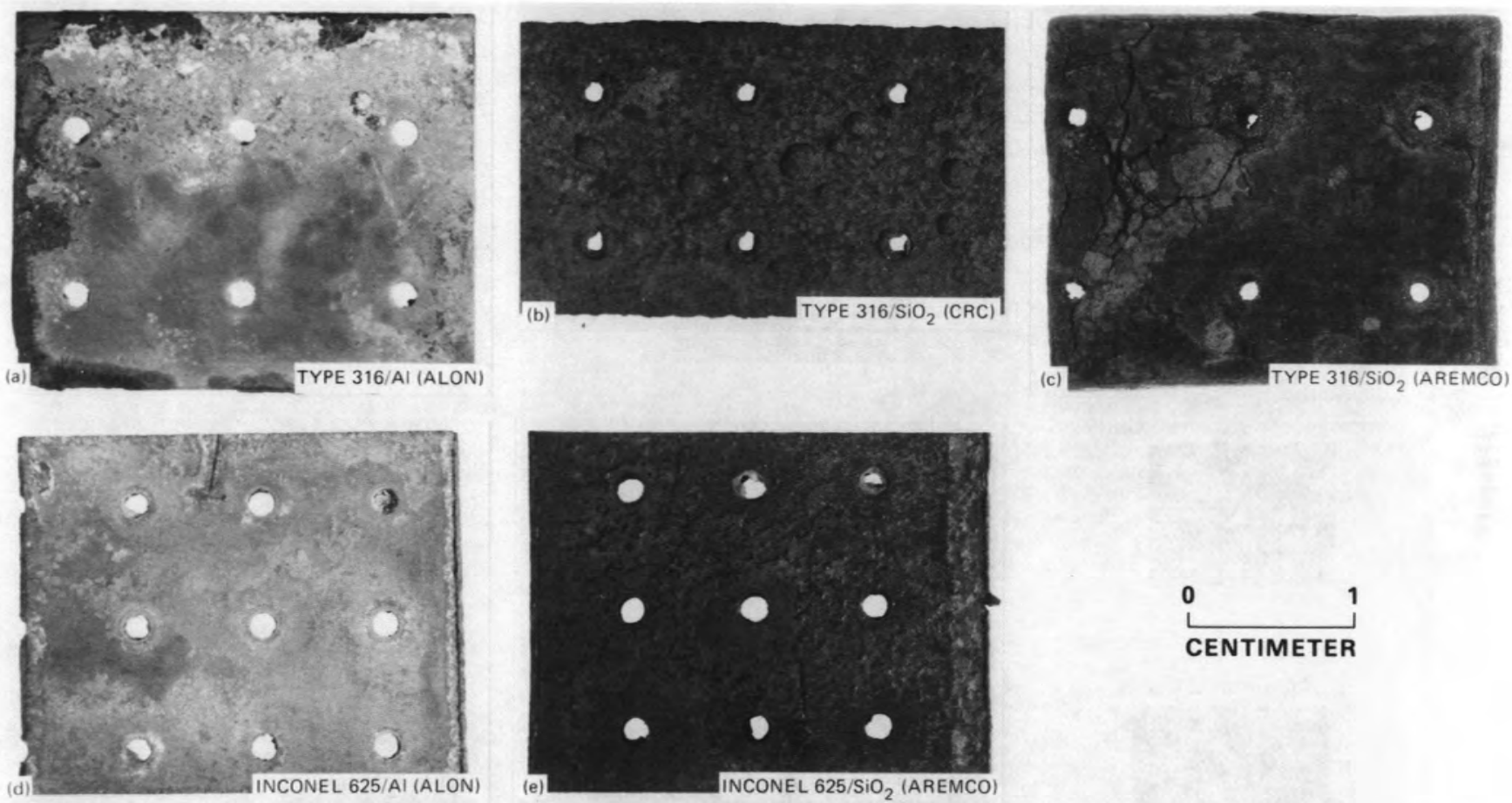

Fig. 16. Coated alloys heat treated at 1000°C for 500 h in air.

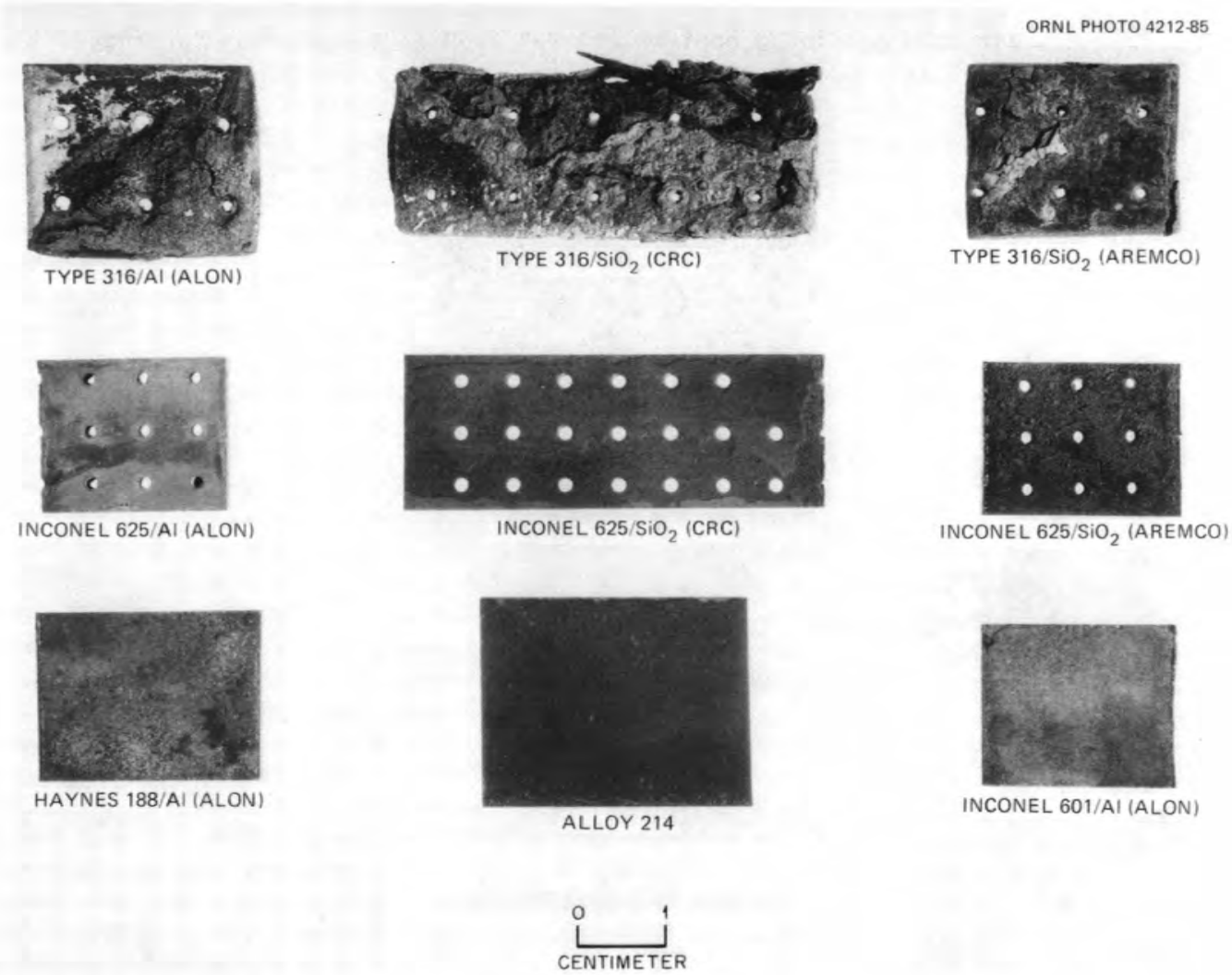

Fig. 17. Coated alloys heat treated at 1000°C for 1000 h in air.

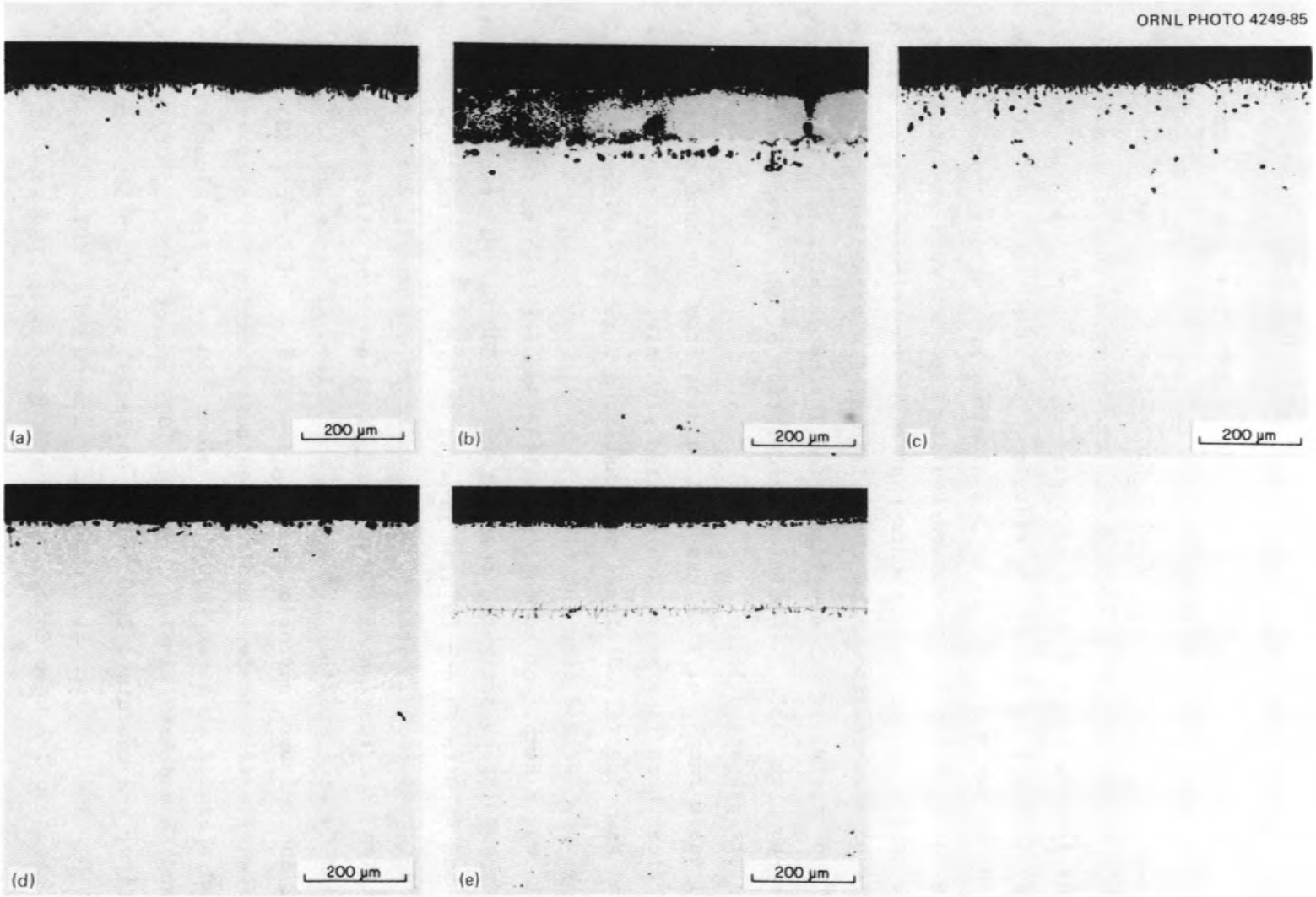

Fig. 18. Microstructures of coated alloys heat treated at 1000°C for 1000 h in air. (*a*) Inconel 625/SiO_2 (Aremco), (*b*) Inconel 625/Al (Alon), (*c*) Inconel 625/SiO_2 (CRC), (*d*) Inconel 601/Al (Alon), (*e*) Haynes 188/Al (Alon). As polished.

ALUMINUM REMELT FURNACE TESTS

Flue Gas Corrosion/Fouling Deposits

The exposure tests were conducted in an aluminum remelt furnace to which a flux was added for purifying the molten aluminum. The composition of the flux was approximately 50 wt % NaCl—45 wt % KCl—5 wt % Na_3AlF_6. Although the flux is mostly confined to the charging zone of the furnace, some flux invariably enters the main part of the furnace and becomes entrained in the flue gases. In addition, the flue gases typically contain elements derived from the molten aluminum and furnace refractories. Flue gas particulates and corrosion/fouling deposits were analyzed, therefore, to determine the constituents that might contribute to corrosion of materials of construction. The compositions of six samples are shown in Table 4 and crystalline phases identified in the samples by X-ray diffraction are shown in Table 5. A brief description of each sample and the analyses are presented below.

V-1 was a sample of flue gas particulates from the hood over the furnace flue where flue gases are diluted with air. Major elements were Cl, K and Na. Identified phases were NaCl and KCl. These compounds evidently were derived from the flux.

V-1A was a sample of corrosion/fouling deposit from an Incoloy 800 sample exposed at an estimated temperature of 1000°C. Major elements were Cr, Fe, and Ni with Zn and Cu also present in high concentrations. Phases were $NiFe_2O_4$ and Fe_2O_3. These results indicate the sample was a product of corrosion or oxidation of the alloy. Zinc, a common alloying element in Al, and Cu were probably present in the molten Al as impurities.

V-2 and V-3 were corrosion/fouling deposits on an Inconel 625 distributor plate of a 1/10-scale fluidized bed test facility. The distributor plate had operated at about 1000°C for about 170 h. Major elements were Cl, K, and Na and both samples contained 1000 ppm or more Al, Cr, and Fe. In addition, V-2 contained 1000 ppm Zn while V-3 contained 5000 ppm Ca, 4000 ppm Mg, and 1000 ppm S. Phases in V-2 were NaCl, KCl, Al_2O_3 and Fe_2O_3; phases in V-3 were $CaSO_4$, NaCl, and MgO. Thus, two samples from the same distributor plate had slightly different compositions and different phases.

Table 4. Composition of flue gas corrosion/fouling deposits

Element	Composition, wt ppm					
	V-1[b]	V-1A[c]	V-2[d]	V-3[d]	V-4[b]	V-5[d]
Al	200	Masked[e]	5000	1000	Major 1[f]	Major 4
As			<3	7	<3	30
B	2	70	200	500	80	200
Ba	20	20	30	300	3000	200
Ca	200	300	400	5000	Major 7	1000
Cd					10	70
Cl	Major	1000	Major	Major	20	100
Co	4	100	<3	3	20	30
Cr	7	Major	1000	3000	700	Major 2
Cs	2					
Cu	30	3000	100	100	1000	800
F	500		2	20		
Fe	70	Major	1000	1000	3000	Major 1
Ga			<2	5	200	30
K	Major	1000	Major	Major	Major 4	700
La			<1	5	20	5
Mg	50		300	4000	200	100
Mn	6	3000	30	70	700	1000
Mo		1000	70	70	5	3000
Na	Major	200	Major	Major	Major 3	400
Nb		600	20	5	20	2000
Ni	100	Major	300	500	300	Major 6
P	6	700	30	50	2000	500
Pb	80				200	30
Rb	50		<1	<1		
S	1000	Masked	200	1000	1000	2000
Sb				3	3	50
Sc				30	30	20
Si	70	Masked	30	500	Major 2	Major 5
Sn				70	30	400
Sr	6	4	10	300	10	50
Ti			10	70	Major 6	800
V	5	70	4	7	50	30
W				70		300
Y			<2	3		
Zn	300	5000	1000	400	Major 5	Major 3
Zr			30	400	40	3000

[a]Spark source spectrographic analyses.

[b]Flue gas particulates.

[c]Corrosion/fouling deposit on Incoloy 800.

[d]Corrosion/fouling deposit on Inconel 625.

[e]Masked means the presence of the element was obscured by another element.

[f]Major means a concentration of several percent or more. In the case of V-4 and V-5 the major elements are given in order of decreasing abundance.

Table 5. Crystalline phases in flue gas corrosion/fouling deposits

Sample	Type	Phases[a]
V-1	Flue gas particulates	NaCl, KCl
V-1A	Corrosion/fouling deposit on Incoloy 800	$NiFe_2O_4$, Fe_2O_3
V-2	Corrosion/fouling deposit on Inconel 625	NaCl, KCl, Al_2O_3, Fe_2O_3
V-3	Corrosion/fouling deposit on Inconel 625	$CaSO_4$, NaCl, MgO
V-4	Flue gas particulates	$ZnAl_2O_4$, Al_2O_3, $Al_6Si_2O_{13}$
V-5	Corrosion/fouling deposit on Inconel 625	$CuCrMnO_4$, Fe_2O_3, $ZnAl_2O_4$

[a]Determined by X-ray diffraction analysis.

V-4 was another sample of flue gas particulates. Major elements in order of decreasing abundance were Al, Si, Na, K, Zn, Ti, and Ca. Other elements present in concentrations of 1000 ppm or more were Ba, Cu, Fe, P, and S. Phases were $ZnO \cdot Al_2O_3$, Al_2O_3, and $3Al_2O_3 \cdot 2SiO_2$.

V-5 was a corrosion/fouling deposit from an Inconel 625 distributor plate after about 3000 h at 1000°C. Major elements in order of decreasing abundance were Fe, Cr, Zn, Al, Si, and Ni. Other elements present in concentrations of 1000 ppm or more were Ca, Mn, Mo, Nb, S, and Zr. Phases were $CuCrMnO_4$, Fe_2O_3, and $ZnAl_2O_4$.

These results show that the flue gases contained various elements derived from the molten aluminum, flux, and furnace refractories. Combination of these elements to form various compounds probably depended on thermal history and concentration. The phases identified by X-ray diffraction generally corresponded to the elements of highest concentrations. Noncrystalline, glassy phases containing various elements were probably also present.

Uncoated and Coated Alloys

Several alloys and ceramic materials were exposed to flue gases in the host aluminum remelt furnace. Inconel 625/Al (TCC) was emphasized in these tests because the alloy was tentatively selected as the interim distributor plate material until a suitable ceramic distributor plate becomes available. The materials and total exposure periods are shown in Table 6. The estimated temperature of exposure was 1000 to 1100°C. Since the furnace operated in a cyclic manner and idled at low temperatures at certain times, such as weekends, the time at elevated temperatures was only about one-third of the total exposure period shown in Table 6.

Microstructures of uncoated Inconel 625 after 2250 and 3230 h total exposure are shown in Fig. 19. Corrosion occurred mainly at grain boundaries to depths of approximately 0.75 and 0.95 mm after 2250 and 3230 h, respectively, which projects to a corrosion rate of 2.8 mm/y (0.1 in./y). Corrosion appears to be much more invasive and destructive than that occurring in air at 1000 and 1100°C as shown in Figs. 9 and 10.

Table 6. Materials and exposure periods in aluminum remelt furnace flue gases

Material	Exposure period (h)
Metallic alloys	
Inconel 625	2250, 3230, 8030
Inconel 625/A	3110
Inconel 625/D	2250, 3230, 4410, 8030
Inconel 601/B	1200
Haynes 188/B	1200, 4030
Alloy 214	1200, 4030
Ceramic materials	
Sintered-α SiC	4300
NC-430 SiC	4300
Refel SiC	4300
Refrax 20 SiC	4300
Alumina	4300
Mullite	4300

ORNL PHOTO 4248-85

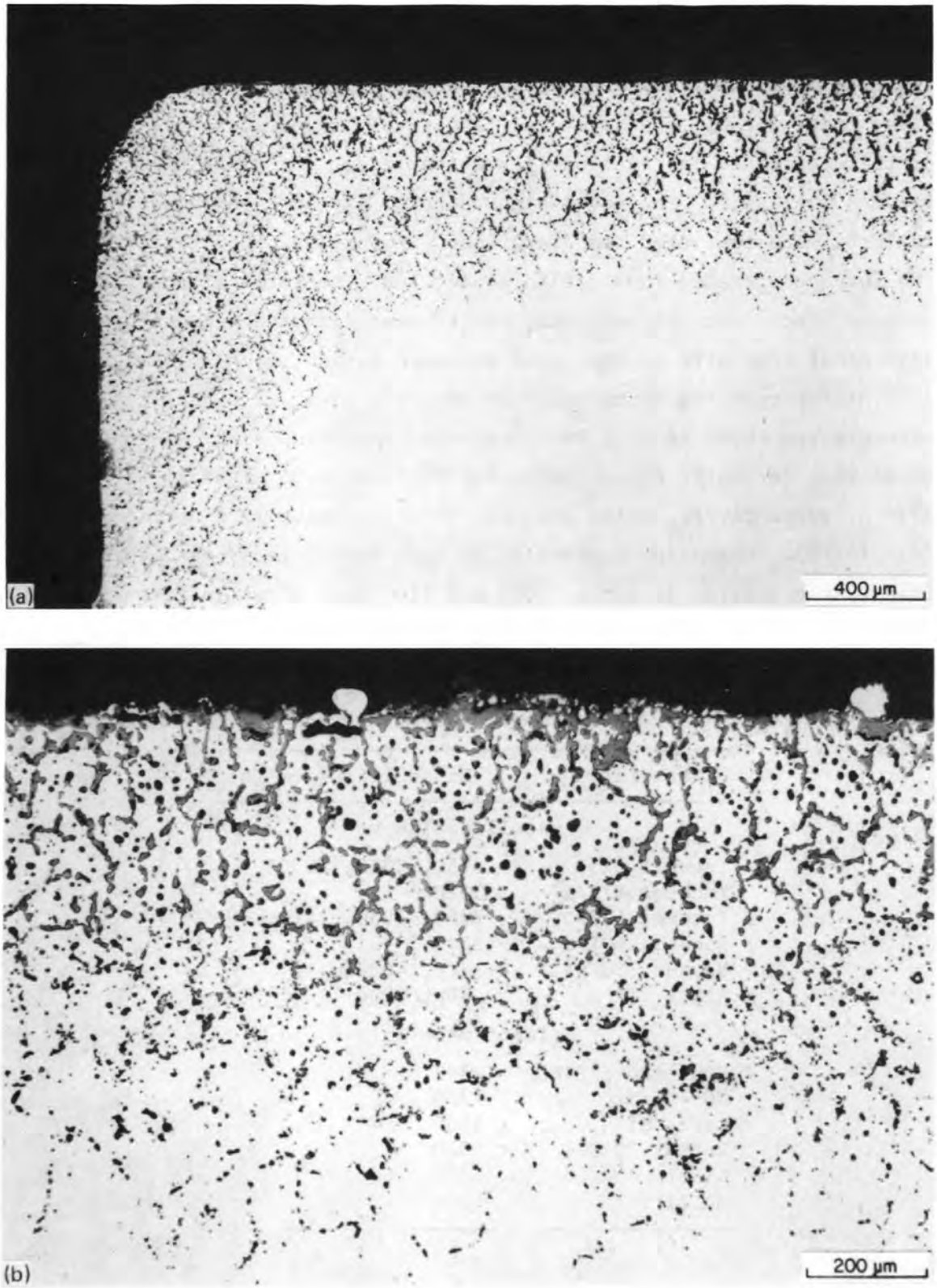

Fig. 19. Uncoated Inconel 625 exposed to flue gases for (*a*) 2250 h, and (*b*) 3230 h. As polished

The load-bearing capability of material in the grain-boundary-affected region is assumed to be seriously decreased relative to the unaffected alloy.

Inconel 625 is normally solution annealed at 1100 to 1200°C to soften the material for cold working and to dissolve minor phases in the matrix. Exposure to lower temperatures (which sometimes occurred) can result in precipitation of carbides containing Ni, Cr, Mo, and Nb (the nominal composition of this alloy was shown in Table 1). Precipitation typically occurs both at grain boundaries and within grains. The corrosion mechanism affecting the material shown in Fig. 19 apparently involved reactions of flue gas constituents with grain boundary precipitates.

Figure 20 shows results of electron microprobe analyses of the specimen shown in Fig. 19(*a*). The BSE image shows a heavy concentration of material in the grain boundaries of the corroded region. The grain boundary material was shown by characteristic X-ray displays (Fig. 20) to contain Cr and O. The implied corrosion mechanism, therefore, is oxidation which preferentially attacks chromium carbides at grain boundaries.

Typical micrographs of Inconel 625/Al (TCC) exposed in the remelt furnace for 2250 h are shown in Fig. 21. The coating was mostly protective, but in some areas corrosion occurred below the coating. Figure 21(*b*) shows an area where the coating protected the substrate on one side, but not the opposite side. The depth of attack was about 0.2 mm (0.008 in.) measured from the outer surface of the coating, which is considerably less than that occurring in uncoated Inconel 625 as previously shown in Fig. 19. The coating also shows degradation in the vicinity of the corroded substrate, as revealed by porosity and/or oxidized material. Another region in the same specimen is shown in Fig. 22 where the coating on the side of a hole has protected the substrate from intergranular attack. The coating has oxidized on the outer surface and pores have formed at the coating/substrate interface.

Other examples of Inconel 625/Al (TCC) exposed for various times are shown in Fig. 23. Intergranular attack had proceeded completely through the thickness of the specimen in one region [Fig. 23(*a*)] but only partly in another region [Fig. 23(*b*)]. Figure 23(*c*) shows intergranular attack proceeding inward from two surfaces. The inconsistent protection by the

ORNL PHOTO 4213-85

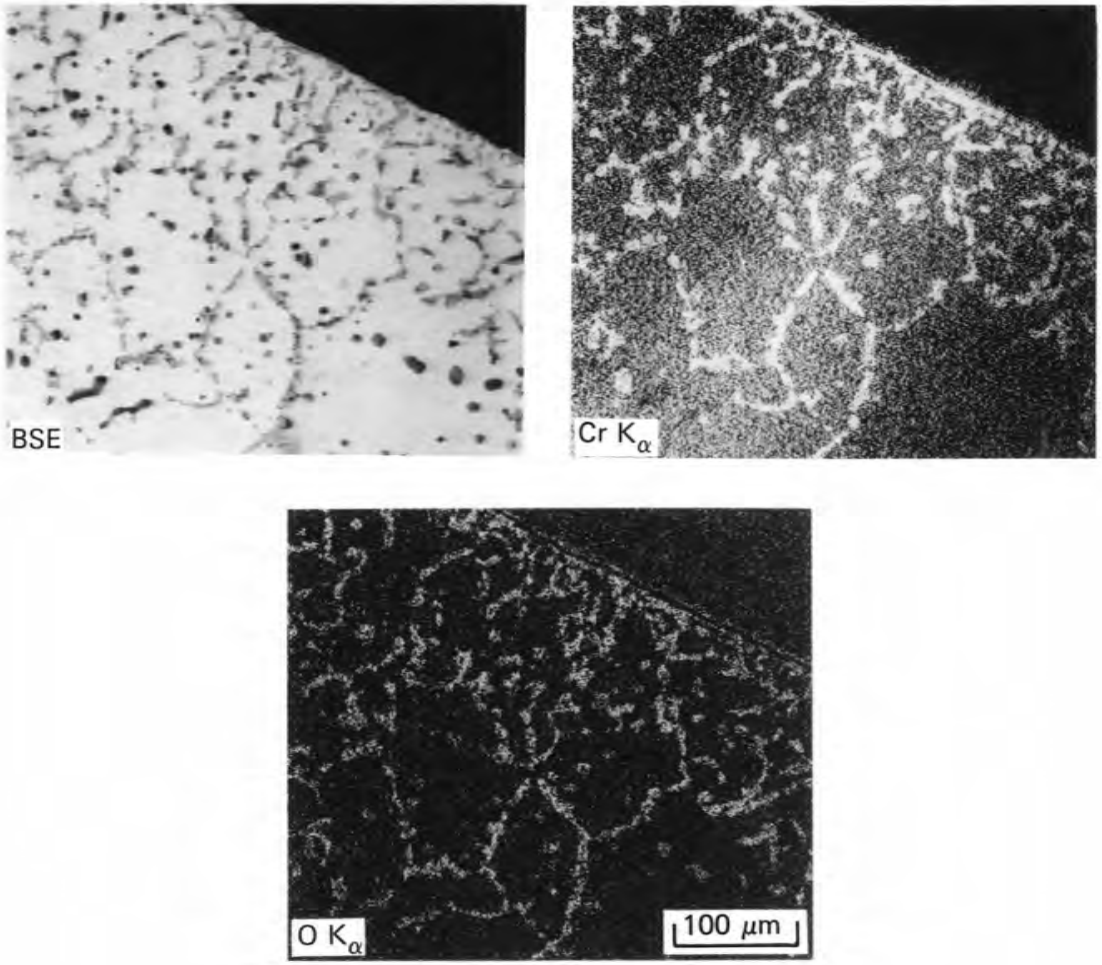

Fig. 20. Characteristic X-ray displays of corroded Inconel 625.

ORNL PHOTO 4247-85

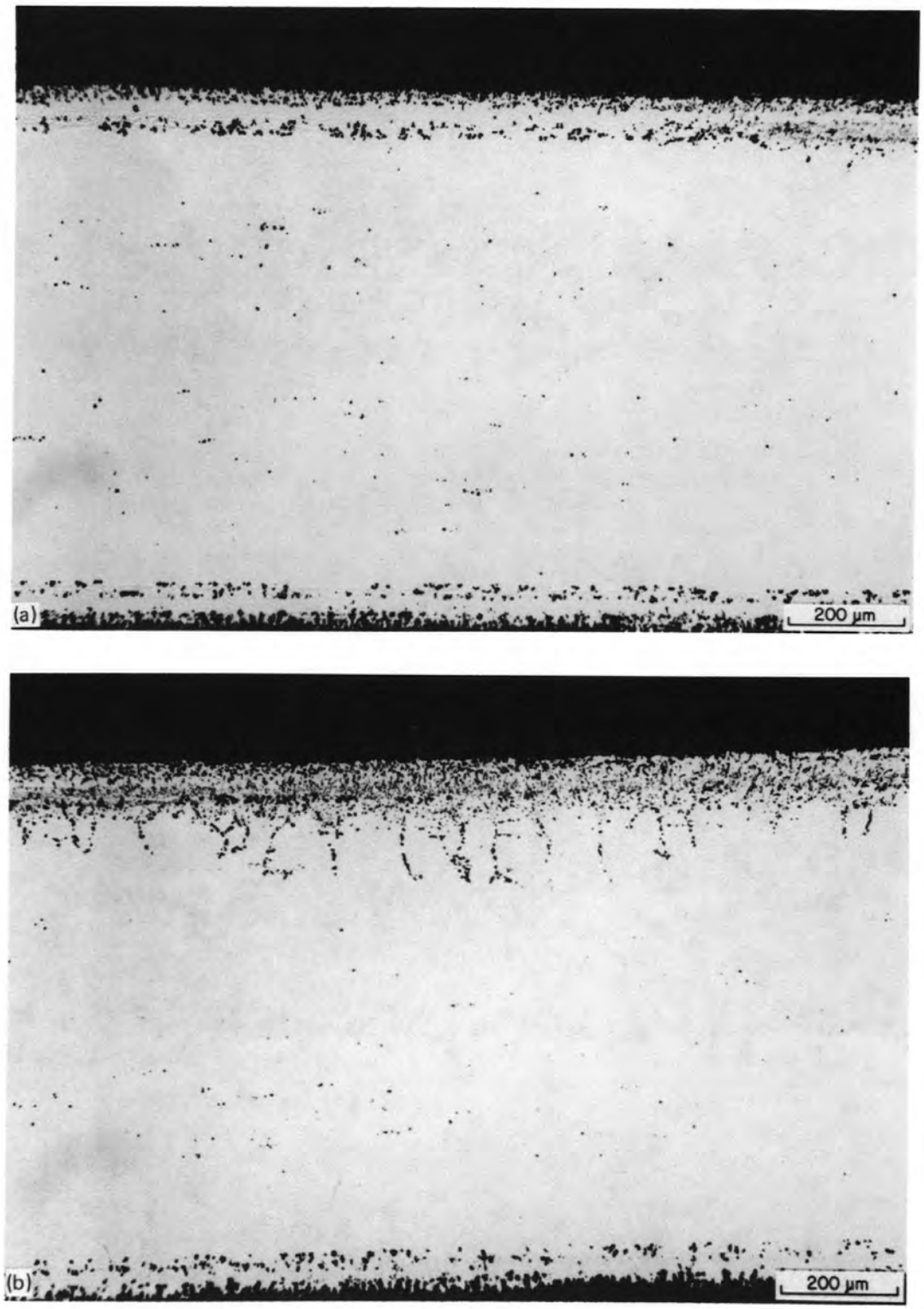

Fig. 21. Inconel 625/Al (TCC) after exposure to flue gases for 2250 h. (*a*) Coating protective on both sides, (*b*) coating protective on one side. As polished.

ORNL PHOTO 4245-85

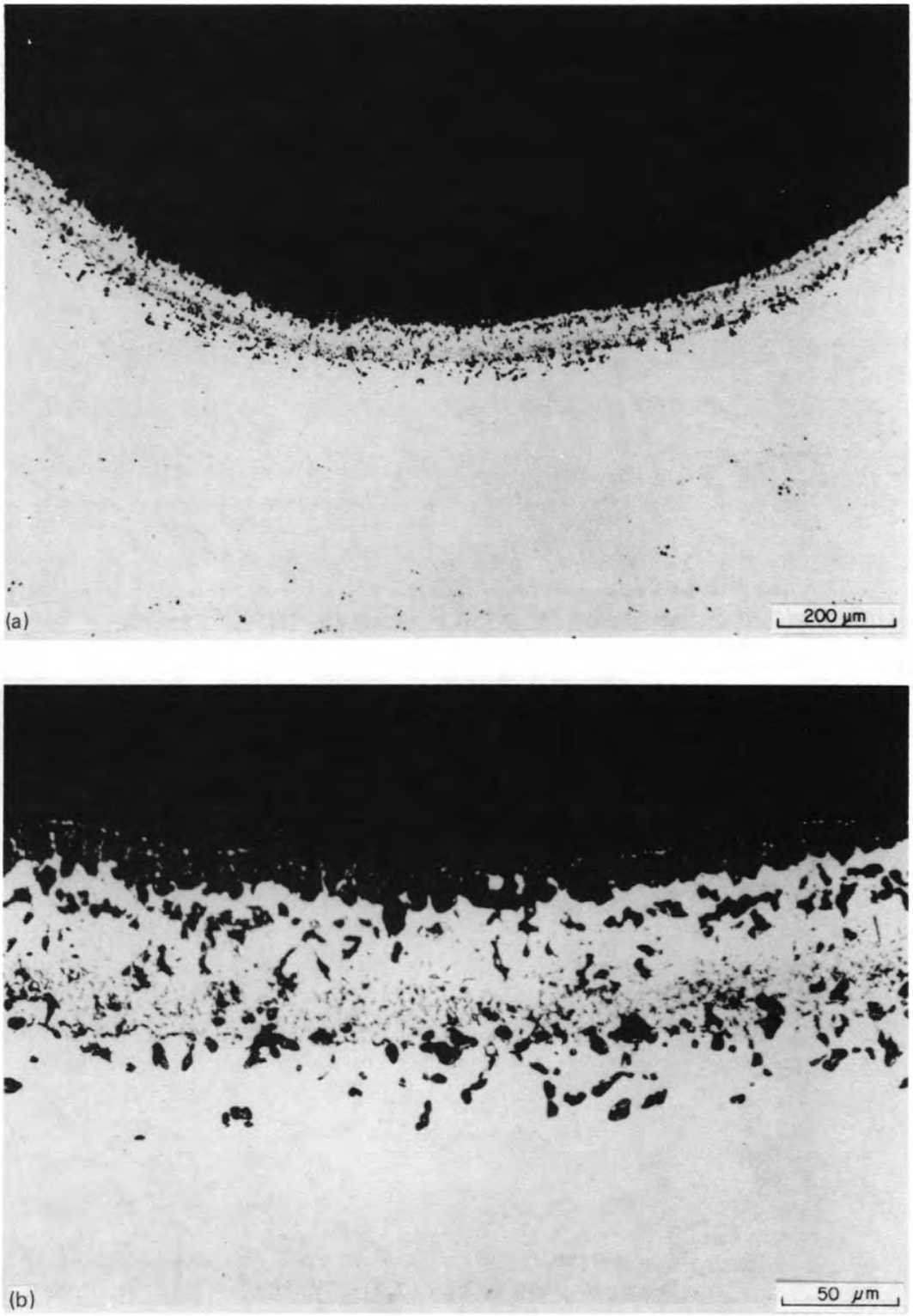

Fig. 22. Inconel 625/Al (TCC) after exposure to flue gases for 2250 h. (*a*) Coating on the side of a hole, (*b*) higher magnification view of the coating. As polished.

ORNL PHOTO 4246-85

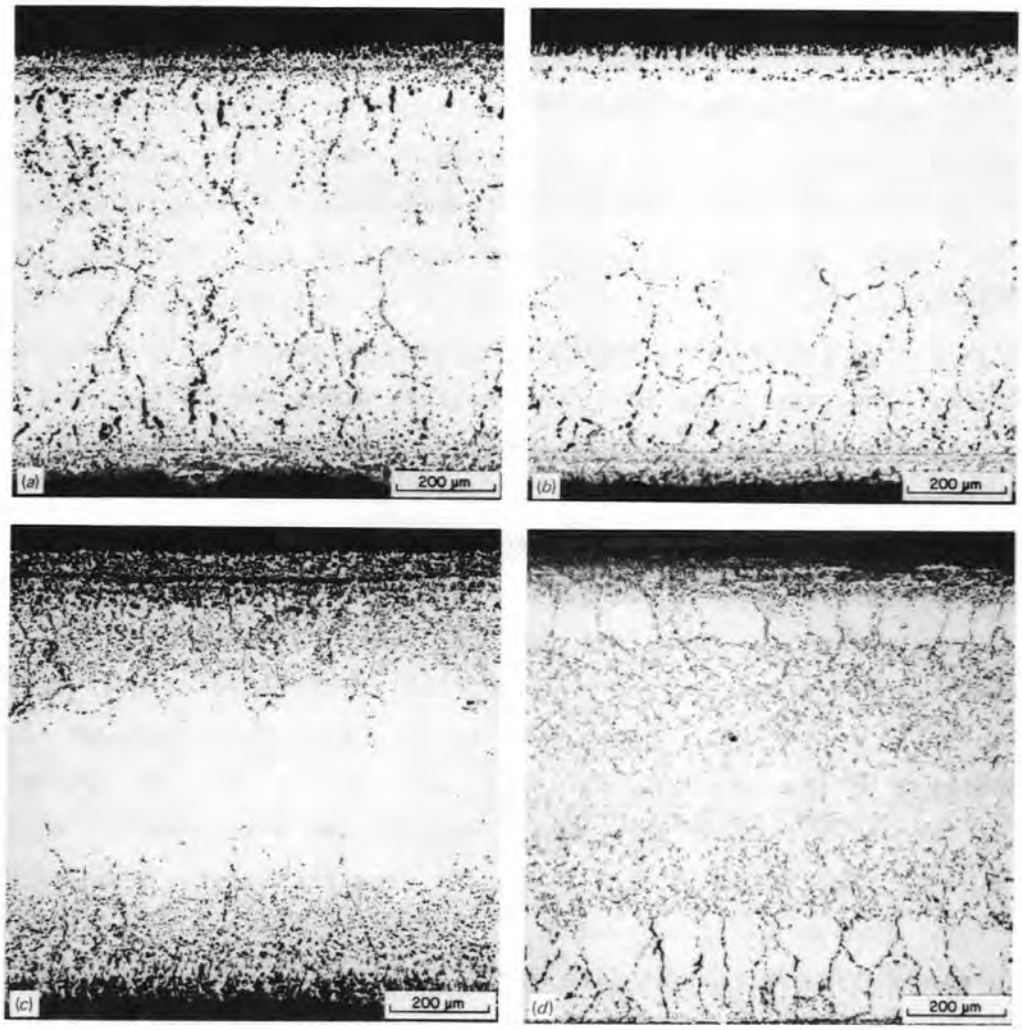

Fig. 23. Inconel 625/Al (TCC) after exposure to flue gases. (*a*) and (*b*) 3230 h, (*c*) 4410 h, (*d*) 8030 h. As polished.

coating might be related to several factors including original coating thickness and diffusion treatment, coating flaws, subsequent exposure to temperature, and severity of thermal cycling.

Electron micrographs show elemental distributions in the coating and substrate. Figure 24 shows a BSE image of coating and substrate. The outer surface of the coating is black and barely distinguishable. Voids or inclusions are visible in the coating and at the interface, and the grain-boundary precipitate is visible in the substrate. The coating was mostly protective in this region, but some corrosion of the precipitate is evident. The oxygen map (O K_α) shows that about one-half of the coating has oxidized and that oxygen is present in the interfacial porosity and the corroded regions of the precipitate. The Mo L_α and Nb L_α maps show that the precipitate contained these elements and that some migration of both elements into the coating has occurred. Figure 25 shows the same BSE image as in Fig. 24. The Fe K_α and Cr K_α maps show that the substrate contains these elements, as expected, that the precipitate is deficient in Fe relative to the grains, and that both Fe and Cr are present in the inner part of the coating. The Al K_α map shows a heavy concentration of Al in the outer part of the coating and a lower concentration on the inner part due to interdiffusion of Fe and Cr from the substrate and Al from the coating. Sodium and zinc, which were shown in Table 4 to be present in high concentration in most flue gas deposits, were also present in the oxidized outer portion of the coating.

These results show that the coating is gradually oxidized in the high temperature combustion environment, the oxidation perhaps enhanced by the presence of elements such as Na and Zn. Oxygen eventually passes through the degraded coating to the substrate, where the primary corrosion process appears to be oxidation of carbides or other grain-boundary precipitates containing Cr, Mo, and Nb. The coating does provide protection to the substrate, but the inconsistent behavior suggests either that the application procedures are not well controlled or that the use temperature and severity of thermal cycling are excessive for the coating.

Other alloys exposed to flue gases in the aluminum remelt furnace are shown in Figs. 26 to 30. Figure 26 shows that Inconel 625/SiO_2 (Aremco)

Y-187459

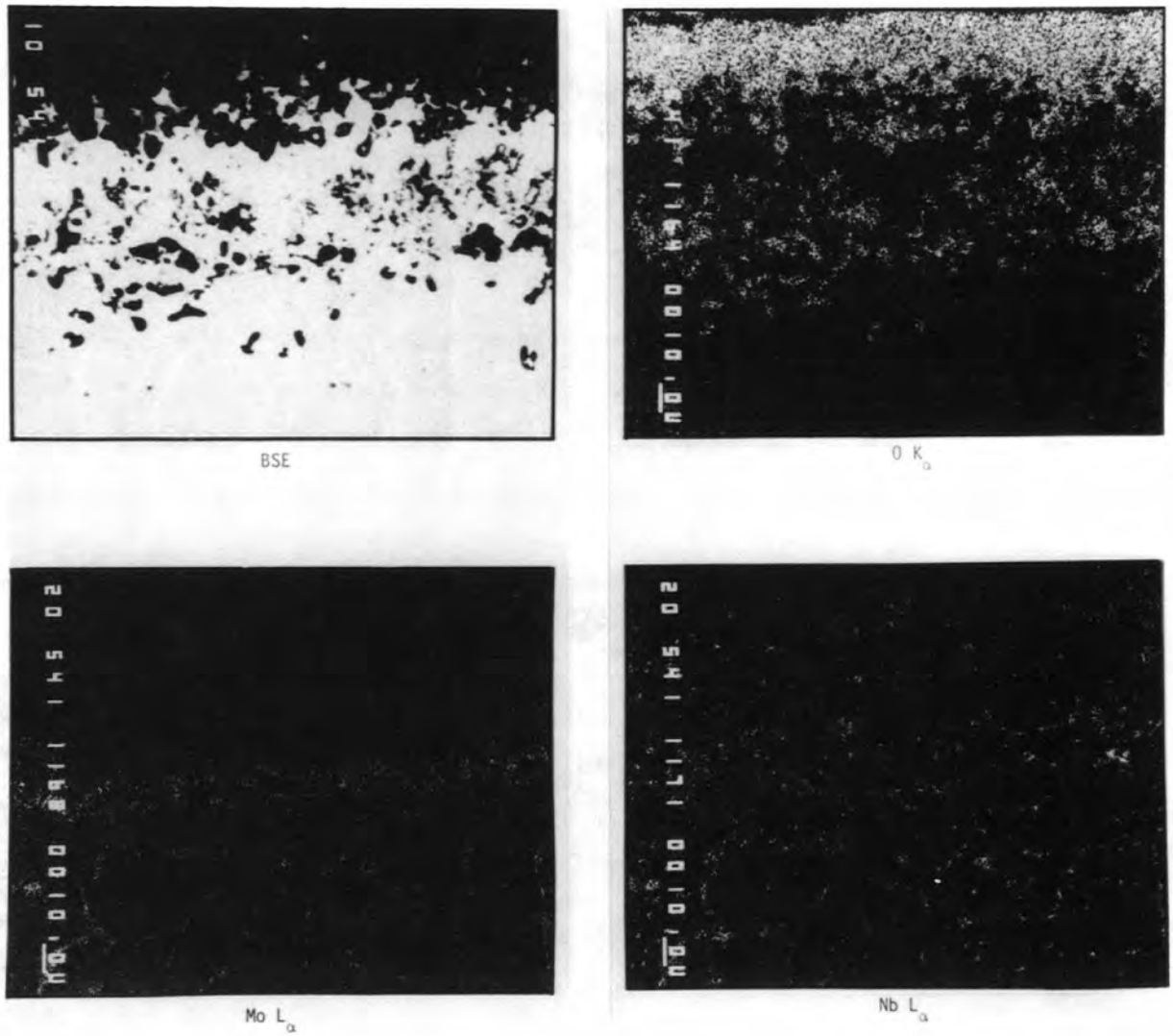

Fig. 24. Characteristic X-ray displays of Inconel 625/Al (TCC) after exposure to flue gases.

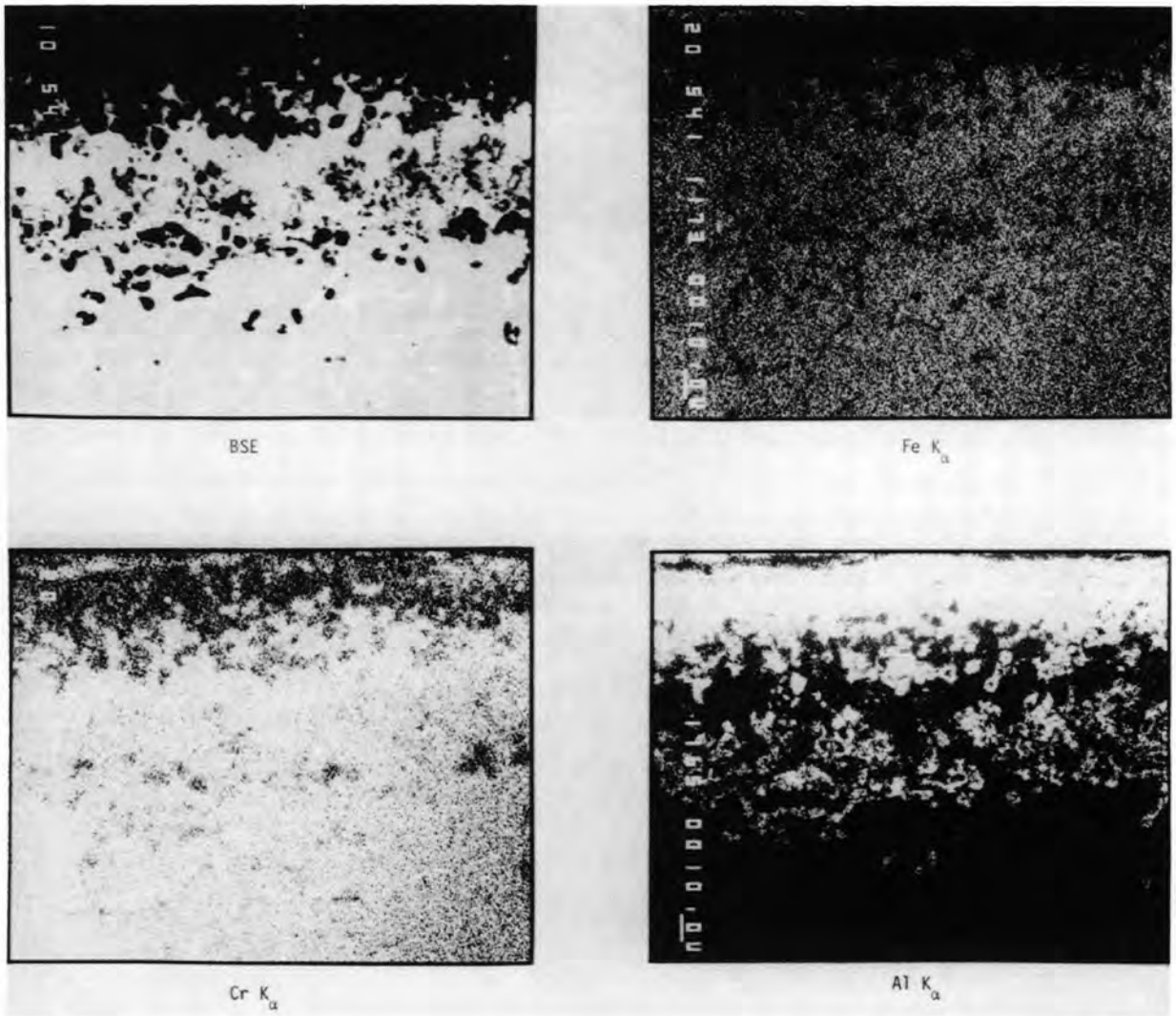

Fig. 25. Characteristic X-ray displays of Inconel 625/Al (TCC) after exposure to flue gases.

ORNL PHOTO 4244-85

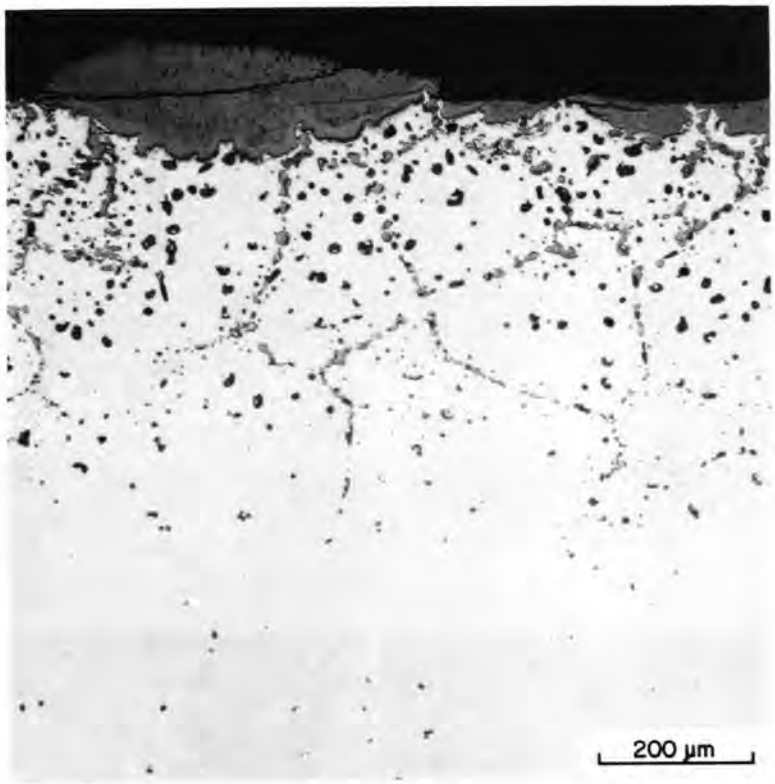

Fig. 26. Inconel 625/SiO_2 (Aremco) after exposure to flue gases for 3110 h. As polished.

exposed for 3110 h was oxidized on the surface, at grain boundaries near the surface, and at isolated regions within near surface grains. The original coating was missing from this sample following the exposure. Figure 27 shows Inconel 601/Al (Alon) after only 1200 h. The coating was missing from one side, where surface oxidation and grain-boundary attack occurred. The coating was degraded, but still intact and protective on the other side. The appearance of Haynes 188/Al (Alon) after 1200 h (Fig. 28) was similar to that of Inconel 601/Al (Alon). After 4030 h further degradation of the coating on Haynes 188/Al (Alon) and more extensive grain-boundary attack had occurred as shown in Fig. 29. Alloy 214 (uncoated) also experienced extensive grain-boundary attack after only 1200 h as shown in Fig. 30.

ORNL PHOTO 4243-85

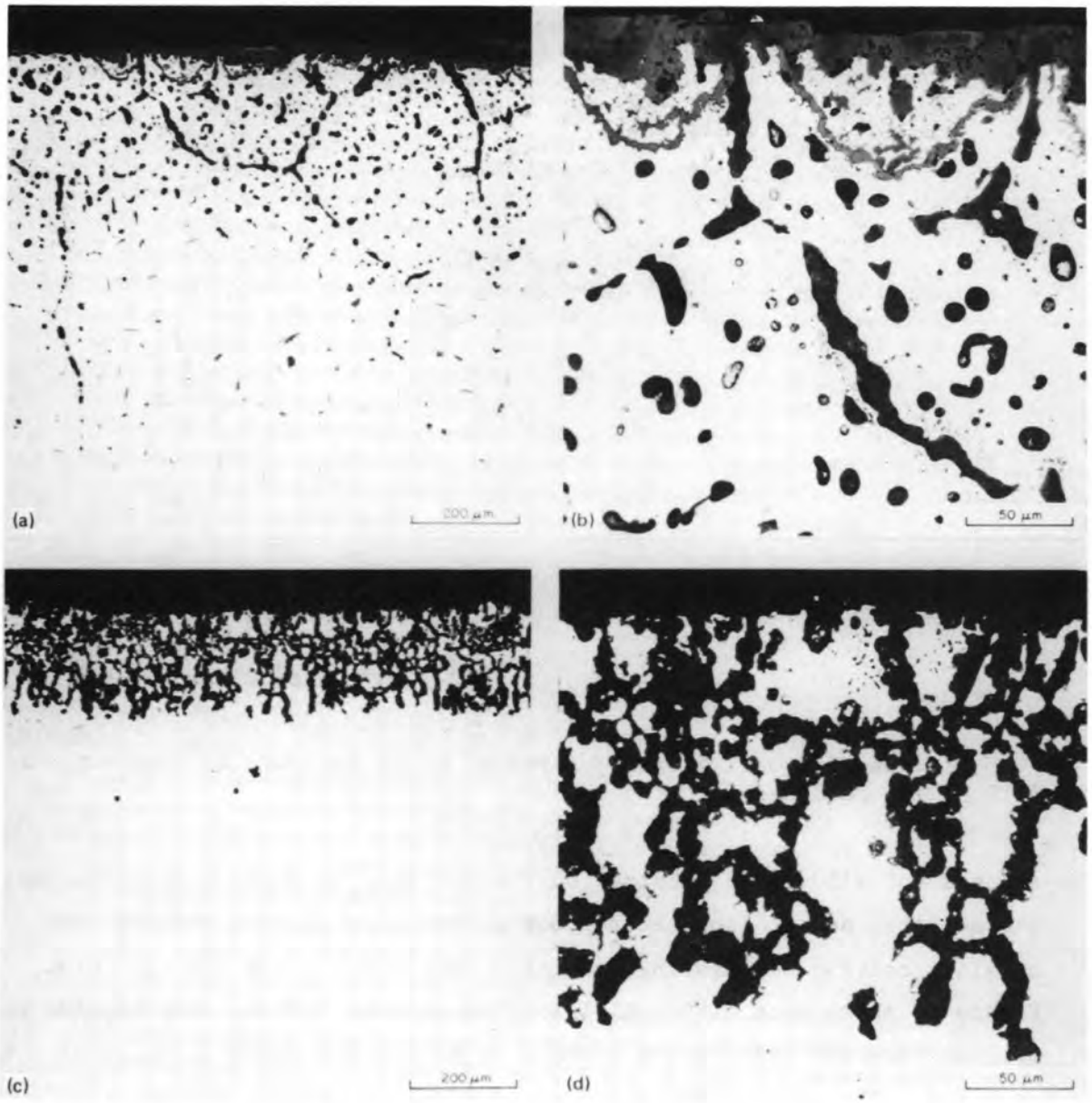

Fig. 27. Inconel 601/Al (Alon) after exposure to flue gases for 1200 h. (*a*) and (*b*) Region where coating was missing, (*c*) and (*d*) region where coating was intact. As polished.

ORNL PHOTO 4242-85

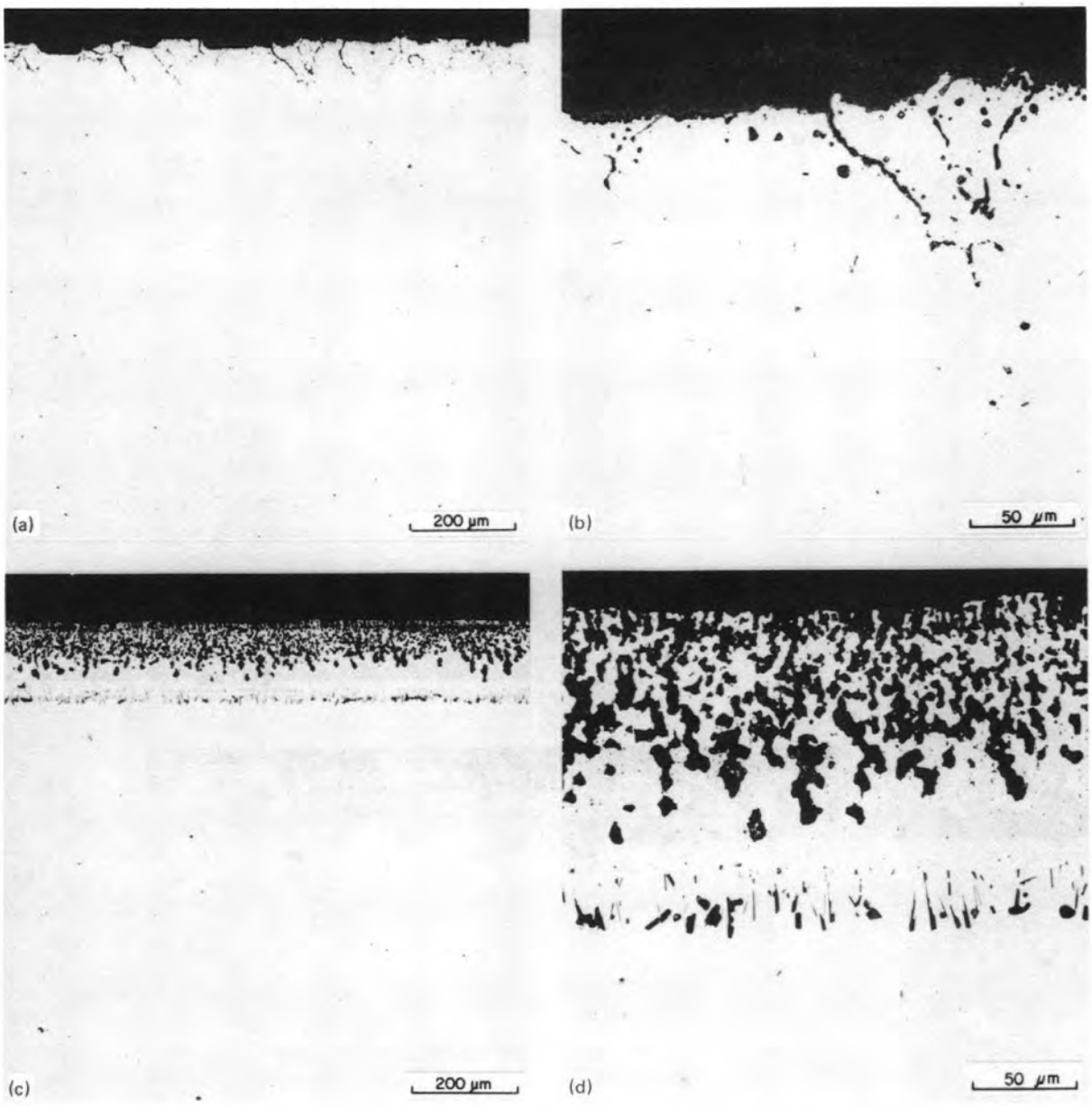

Fig. 28. Haynes 188/Al (Alon) after exposure to flue gases for 1200 h. (*a*) and (*b*) Coating missing, (*c*) and (*d*) coating intact. As polished.

ORNL PHOTO 4241-85

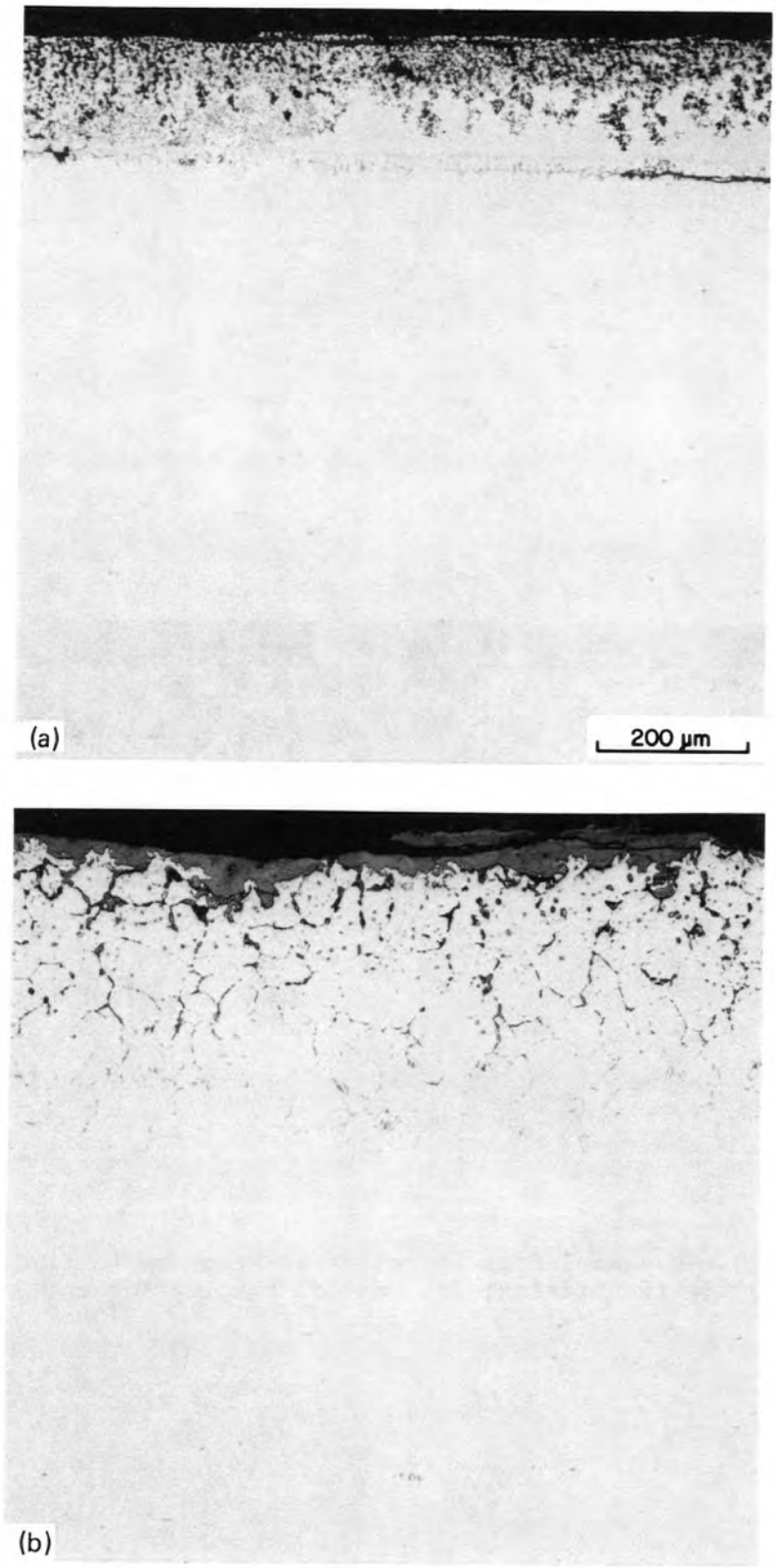

Fig. 29. Haynes 188/Al (Alon) after exposure to flue gases for 4030 h. *(a)* Coating intact, *(b)* coating missing. As polished.

ORNL PHOTO 4240-85

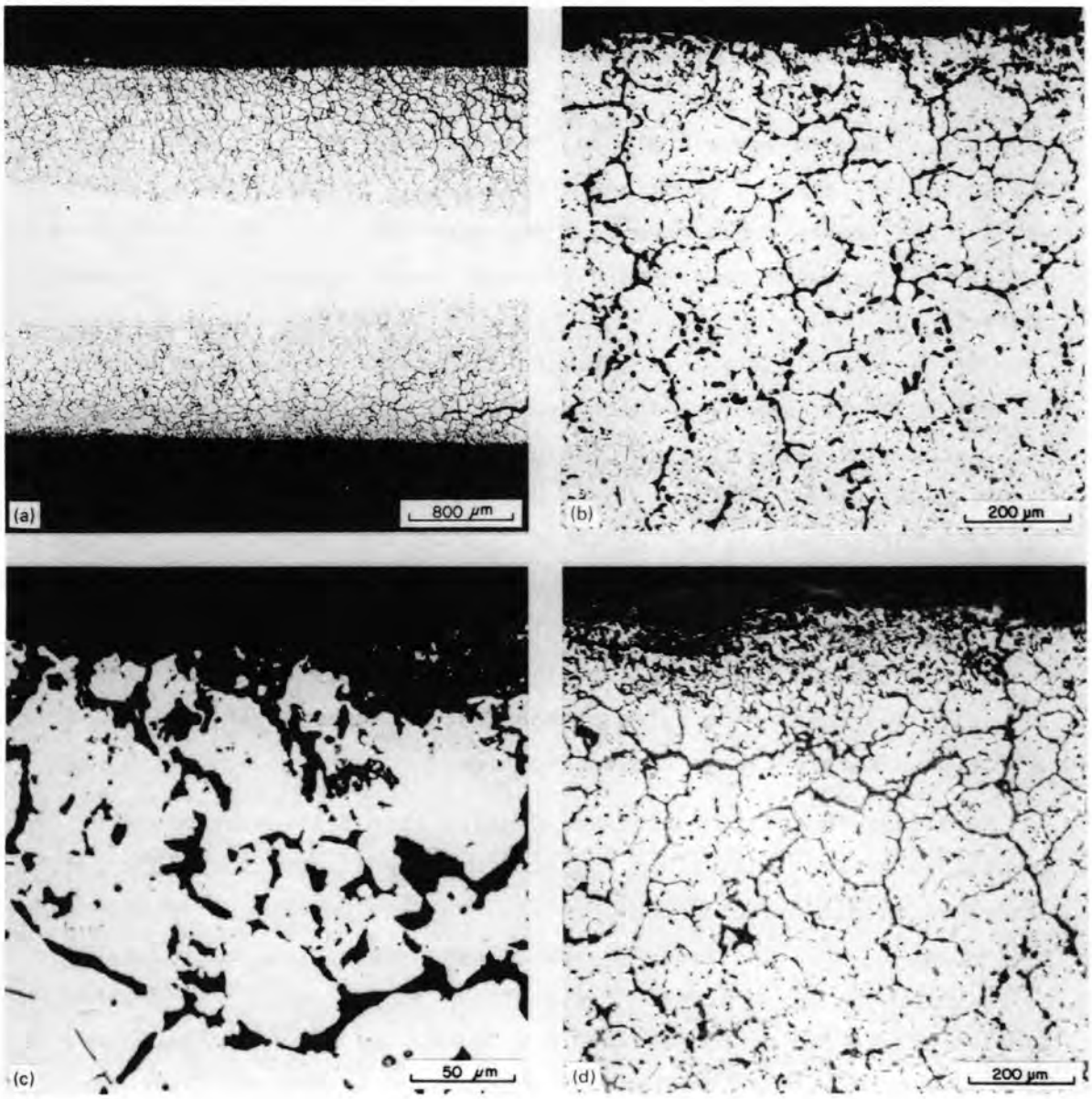

Fig. 30. Uncoated Alloy 214 after exposure to flue gases. (*a*), (*b*), and (*c*) 1200 h, (*d*) 4030 h. As polished.

As shown by preceding micrographs of corroded alloys, grain-boundary attack typically occurred during remelt furnace exposure. Measurement of the depth of grain-boundary attack allows the lifetime of a component of known thickness to be approximately predicted. Table 7 shows the maximum depth of attack in various alloys, the corrosion rate based on the total exposure time, and the projected annual rate. If the furnace had operated at elevated temperatures more than one-third of the total time (as in this work), the corrosion rates would probably have been higher. The data indicate the following:

- if the anomalously low corrosion rate for uncoated Inconel 625 at 8030 h is ignored, this material corroded faster than Inconel 625/SiO_2 (Aremco), which, in turn, corroded faster than Inconel 625/Al (TCC);
- the corrosion rates of uncoated Inconel 625, Haynes 188/Al (Alon) and uncoated Alloy 214 decreased with time, which would be expected if corrosion rates are controlled by diffusion; and
- the corrosion rate of Alloy 214, which exhibited minimal oxidation in air, was equal to or higher than that of several other alloys for approximately the same exposure time.

Previous investigations have revealed that high temperature alloys are severely attacked in aluminum remelt furnace environments. An exposure of stainless steels and nickel-base alloys to flue gases yielded high recession rates.[6] Tube specimens of the alloys were cooled internally with air to maintain the outer surfaces at desired temperatures. The stainless steels were tested at 650 and 815°C for 1000 and 1300 h at each temperature, while the nickel-base alloys were tested at 815 and 925°C for the same periods. Projected annual corrosion rates for the stainless steels varied considerably, but were generally higher at the lower temperature (6.7—12.1 mm/y vs 1.8—3.4 mm/y) apparently due to the corrosive effect of Na_2SO_4. At about 650°C Na_2SO_4 is highly fluid and corrosive, whereas the higher vapor pressure of the compound minimized its contact with the specimens at 815°C. Projected annual corrosion rates for the nickel-base alloys were within the approximate range 2.5 to 5.1 mm/y. These high corrosion rates indicated that the flue gases in this particular furnace were extremely aggressive to many high temperature alloys.

Table 7. Corrosion rates of materials exposed to aluminum remelt furnace flue gases at 1000 to 1100°C

Material	Total exposure time,[b] h	Maximum depth of attack[a] (mm)	Corrosion rate (nm/h)	Projected corrosion rate [mm/y (in./y)]
		Metallic alloys		
Inconel 625	2250	0.76	340	3.0 (0.12)
	3230	1.04	320	2.8 (0.11)
	8030	0.25	30	0.3 (0.01)
Inconel 625/ Al (TCC)	2250	0.20	90	0.8 (0.03)
	3230	0.46	140	1.2 (0.05)
	4410	0.46	*c*	*c*
	8030	0.46	*c*	*c*
Inconel 625/ SiO_2 (Aremco)	3110	0.56	180	1.6 (0.06)
Inconel 601/ Al (Alon)	1200	0.71	590	5.2 (0.20)
Haynes 188/ Al (Alon)	1200	0.20	170	1.5 (0.06)
	4030	0.41	100	0.9 (0.04)
Alloy 214	1200	1.02	850	7.4 (0.29)
	4030	1.27	320	2.8 (0.11)
		Ceramic materials		
Sintered-α SiC	4300	0.30	70	0.6 (0.02)
NC-430 SiC	4300	0.25	60	0.5 (0.02)
Refel SiC	4300	0.25	60	0.5 (0.02)
Refrax 20 SiC	4300	*d*		
Alumina	4300	0	0	0
Mullite	4300	0.08	19	0.2 (0.01)

[a]Depth of grain boundary attack in alloys. Depth of reaction zone in ceramic materials.

[b]Since furnace was operated in a cyclic manner and idled at low temperatures on weekends, the time at elevated temperature was only about one-third of the total exposure time.

[c]Depth of grain boundary attack equal to one-half specimen thickness during previous exposure period (3230 h).

[d]Not measured.

Another investigation involved corrosion of a radiant recuperator on an aluminum remelt furnace.[7] The type 309 stainless steel inner shell of the recuperator was extensively corroded after only about 35 d of operation. During this time one or more high temperature excursions might have accelerated corrosion. Corrosion was characterized by extensive surface scale formation and intergranular attack of the alloy directly under the scale. In some areas the 5-mm-thick radiant insert was completely consumed by corrosion. Electron microprobe analyses revealed Cl, K, and S in the grain boundary corrosion product. The cause of corrosion was attributed to both sulfidation-oxidation and to attack by chlorides.

Another investigation under controlled conditions was conducted to study the effects of halides on high temperature corrosion of stainless steels and nickel-base alloys.[8] In this work the specimens were alternately dipped in an aqueous halide solution of NaCl, NaI, NaBr, or NaF, then heated to 800 to 1000°C in air. The specimens exhibited destructive scale formation and internal oxidation (or grain boundary attack) resulting in typical corrosion rates of 25 μm/h (0.001 in./h). Investigation showed that the halides were more corrosive when the exposure temperature was above their melting points. The corrosion was attributed to the halide species because tests with compounds such as NaOH and $NaHCO_3$ showed that sodium ions did not enhance corrosion.

The results of the present investigation, therefore, are in general agreement with those of other investigators who have observed severe corrosion of metallic alloys in high temperature halide-containing flue gases. Another factor that might significantly increase corrosion rates in a fluidized bed is the eroding action of bed media. Erosion might continually remove oxide or corrosion layers, thereby exposing fresh surfaces to attack by the environment.

CERAMIC MATERIALS

Corrosion rates for SiC ceramics and two oxide ceramics are also shown in Table 7. The data show that the SiC ceramics had substantially more surface recession and higher projected corrosion rates than the oxide ceramics. Sintered-α and two siliconized SiC ceramics (NC-430 and Refel)

had similar corrosion rates of about 0.5 mm/y (0.02 in./y). Corrosion in Refrax 20 was indicated ceramographically, but surface recession was not actually measured.

Microstructures of the sintered-α and NC-430 SiC ceramics are shown in Fig. 31. Both specimens had a glassy layer on the surface which contained several types of crystals and some large gas bubbles. The surfaces of both specimens were rough, indicating that corrosion had occurred. Electron microprobe analyses revealed that the glass on the sintered-α specimen [Fig. 31(*a*), (*b*)] contained high concentrations of Al and Ca and substantial amounts of Fe, K, Mg, Si, and Zn. The light crystals in the glass contained Mg, Ni, and Si, while the dark crystals contained Al and Si. Nickel was also strongly concentrated at the interface. The glass on the NC-430 specimen [Fig. 31(*c*), (*d*)] contained K, Al, Ca, and Si. Particles at the interface contained high concentrations of Fe, Ni, and Cu. Glass has penetrated into the specimen via the free Si phase to a depth of about 300 μm.

Other investigators have observed Fe and Ni at the SiC-slag interface. Ferber and Tennery first reported this phenomenon in their study of reactions between SiC ceramics and coal slag.[9,10] They suggested that the corrosion process involved formation of Fe-Ni-Si compounds. In another study particles containing high concentrations of Fe and Ni were present at the SiC-slag interface after exposure to a steel soaking pit environment.[11,12] The observation in this work of phases containing Ni or Fe, Ni, and Cu at the SiC-slag interface is consistent with the results of previous studies. This consistency in results suggests that similar corrosion mechanisms have occurred in the various furnace environments.

Another siliconized SiC (Refel) is shown in Fig. 32(*a*). The specimen of this material was characterized by nonuniformity of microstructure. Considerable variation in the free SiC content can be seen. The crack near the surface of the sample might have occurred during cutting for examination. The surface of the specimen was covered with a glass containing a few crystals and large bubbles, the latter indicating a reaction involving formation of gas. Corrosive attack was uniform, i.e., neither SiC nor Si at the surface was selectively attacked.

ORNL PHOTO 4214-85

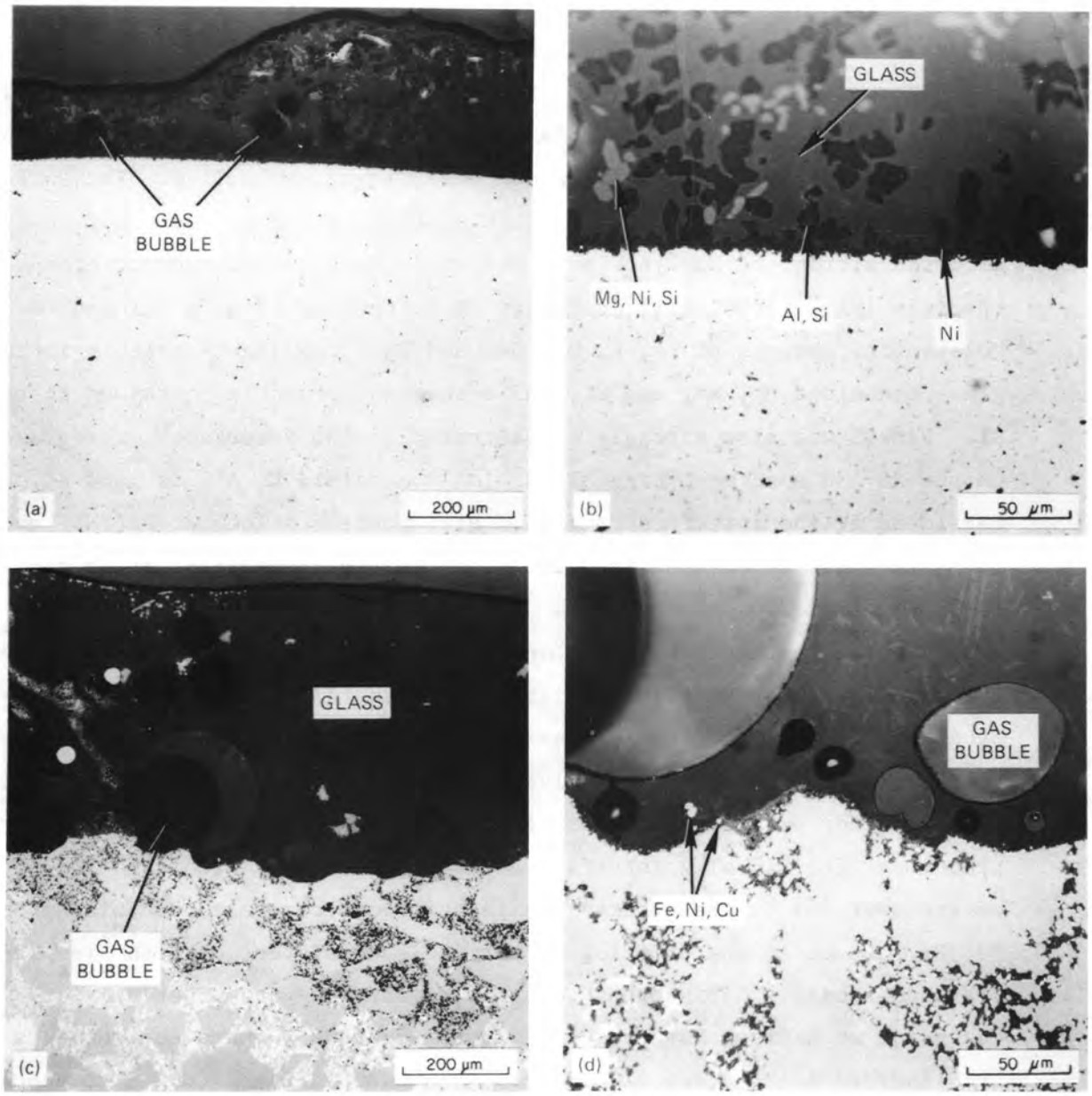

Fig. 31. Sintered-α and NC-430 SiC ceramics after exposure to flue gases for 4300 h. (*a*) and (*b*) Sintered-α, (*c*) and (*d*) NC-430. As polished.

ORNL PHOTO 4216-85

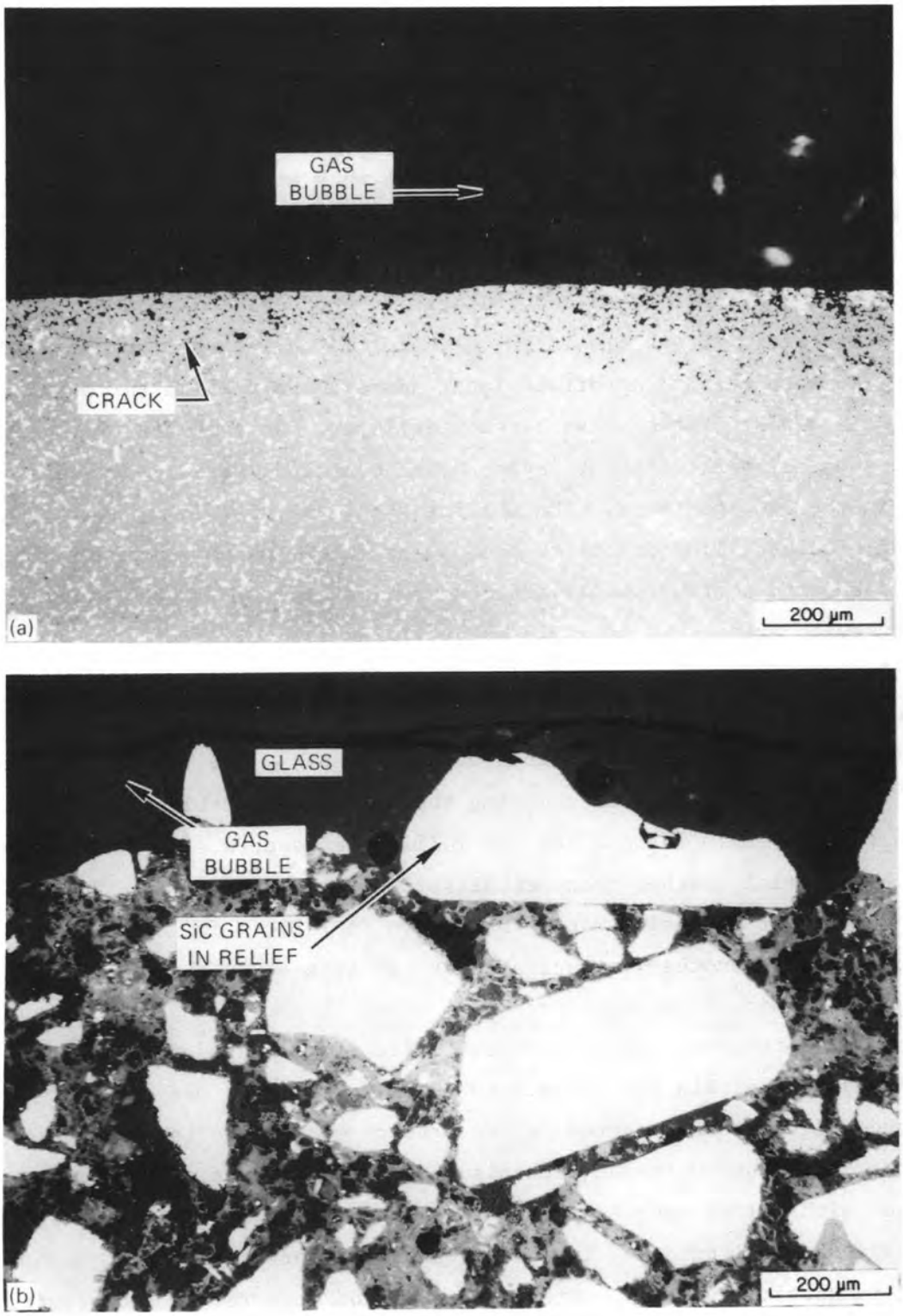

Fig. 32. SiC ceramics after exposure to flue gases for 4300 h. (*a*) Refel SiC, (*b*) Refrax 20. As polished.

Figure 32(*b*) shows a typical region in the Si_3N_4-bonded SiC (Refrax 20). The glass coating on the surface has reacted with the Si_3N_4 matrix phase resulting in relatively corrosion-resistant SiC grains being left in relief. Gas bubbles are also evident in the glass, indicating a reaction-forming gas. Close examination also reveals that the SiC grains are being attacked, although much more slowly than the matrix.

Typical regions in the oxide ceramics are shown in Fig. 33. The alumina specimen [Fig. 33(*a*) and (*b*)] exhibits the closed porosity typical of this material. Some pores might have formed during specimen preparation. The specimen had a surface layer approximately 25 μm thick, which might be a deposit rather than a reaction layer. No evidence of reaction can be seen below the deposit layer, which contained various elements found in the SiC specimens. The mullite specimen [Fig. 33(*c*) and (*d*) had a layer of crystalline deposits about 50 μm thick, which contained Al, Fe, Ni, and Zn, and a structurally affected region about 75 μm thick. The latter region appears to be a glass containing randomly distributed crystals containing Al, Fe, and Ni. The mullite has evidently reacted with constituents of the flue gases (such as NaCl, KCl, and SiO_2) to form a silicate glass containing various other elements. The crystals in the glass might have formed either during the exposure or cooling. The corrosion rate shown in Table 7 for the mullite represents structurally affected material, rather than actual surface recession.

Much higher corrosion rates than shown in Table 7 for SiC ceramics were obtained in another investigation.[6] In this study specimens were exposed to aluminum remelt furnace flue gases at about 1100°C for about 2450 h. The projected annual corrosion rates (calculated from the data in ref. 6) were within the range 3 to 10 mm/y, or about one order of magnitude higher than observed in the present work. The investigators suspected that the corrosion mechanism involved reaction of the SiC ceramics with halide species in the flue gases to form volatile silicon halides and alkali oxides. In another study of corrosion of SiC ceramics in six industrial furnaces, extensive corrosion occurred in two aluminum remelt furnaces and a steel soaking pit.[12] Corrosion rates in one aluminum remelt furnace projected to 0.1 to 0.6 mm/y (0.004–0.024 in./y).

ORNL PHOTO 4215-85

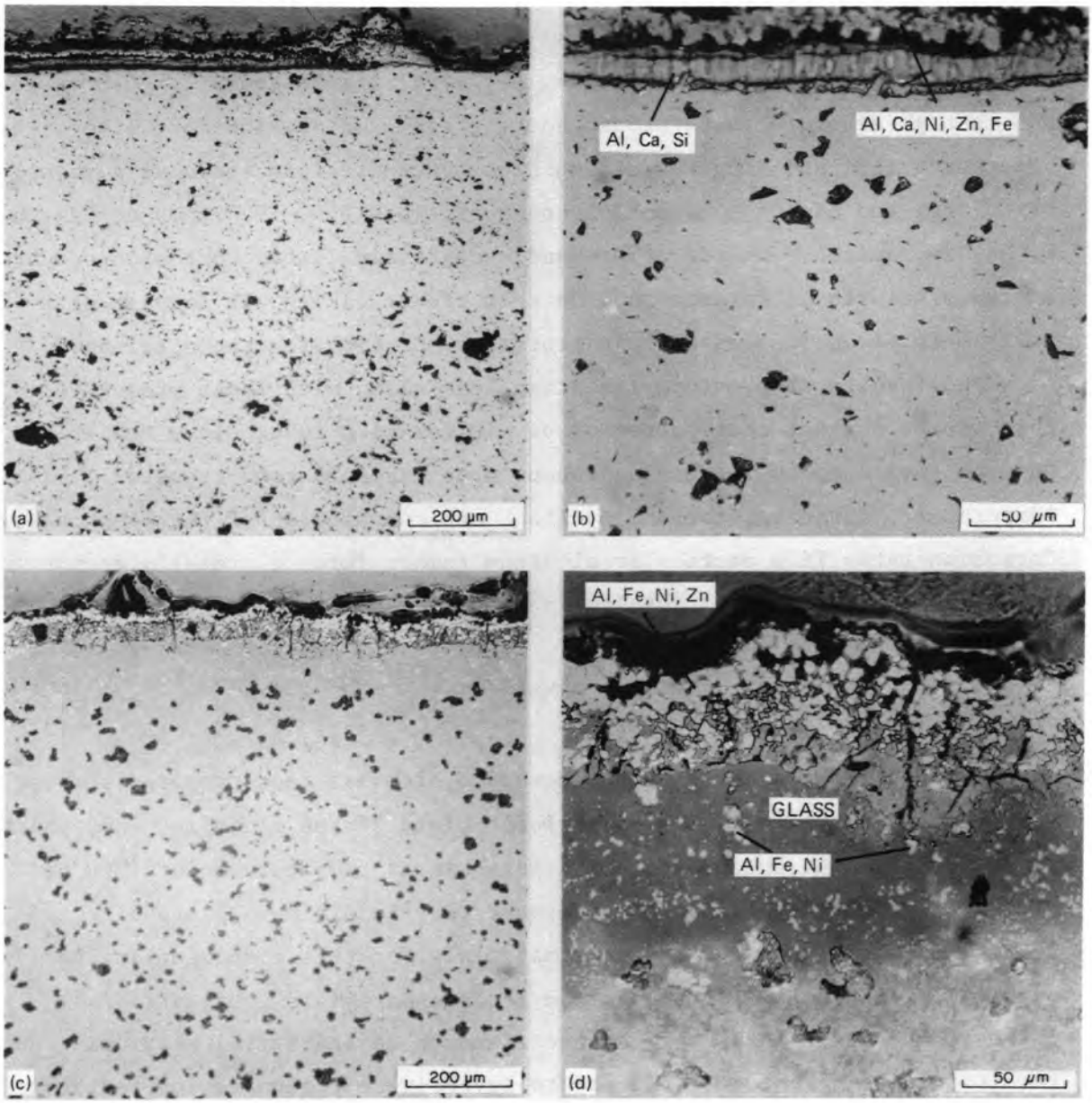

Fig. 33. Oxide ceramics after exposure to flue gases for 4300 h. (*a*) and (*b*) AD-998 alumina, (*c*) and (*d*) mullite. As polished.

Corrosion rates in the other aluminum remelt furnace (the same furnace in which the present work was conducted) were even higher, but, because the exposure time was only 530 h, annual corrosion rates were not projected. Corrosion rates in the steel soaking pit were still higher (3.5–6.8 mm/y) due to high exposure temperatures and the combined erosion-corrosion of an aggressive silicate slag containing high concentrations (several percent) of Cr, Fe, and Si and substantial concentrations (500–3000 ppm) of Ca, Cu, K, Mn, Na, and Ni. On the other hand, relatively little corrosion occurred in two steel reheat furnaces and another steel soaking pit because of relatively clean flue gases or a protected location for the specimens.

The results of previous investigations along with those presented in this report suggest that corrosion of SiC ceramics in aluminum remelt furnace environments is very dependent upon exposure conditions of temperature, duration, thermal cycling, and composition of the flue gases. Corrosion rates in a particular aluminum remelt furnace probably cannot be predicted accurately from results in another furnace.

SUMMARY

A fluidized bed waste heat recovery system has been proposed for use on industrial furnaces. The distributor plate of the fluidized bed, which will be exposed to the combustion atmosphere at temperatures of 1000 to 1100°C, must be strong enough to support the fluidizing media and resistant to corrosion. Candidate materials for this component include high temperature metallic alloys and ceramic materials. Oxidation/corrosion tests in laboratory furnaces and in an industrial aluminum remelt furnace have been conducted to investigate the corrosion resistance of candidate materials. Eleven Fe-, Ni-, and Co-base alloys were tested: type 316, 310, and 446 stainless steels; Incoloy 800; Inconel 601 and 625; Hastelloy N and X; Haynes 25 and 188; and Alloy 214. Some alloys were also tested with Al or SiO_2 coatings applied by commercial suppliers. Four SiC ceramics (sintered-α, NC-430, Refel, and Refrax 20) and two oxide ceramics (AD-998 alumina and mullite) were also tested. Specimens of the

alloys were tested at 1000°C (1000 h) and 1100°C (1136 h) in air in laboratory furnaces. Some of the alloys and the ceramic materials were tested in an aluminum remelt furnace at 1000 to 1100°C for up to 8030 h.

Some as-fabricated aluminum coatings were dense and adherent. Some had a diffusion zone at the coating-substrate interface. Some aluminum coatings were cracked or had porosity at the interface. Some SiO_2 coatings were poorly formed and porous, while others appeared to be relatively dense and adherent. The number of coated specimens was insufficient to relate the quality of the coatings to either the substrates or the manufacturers.

In air oxidation tests at 1000°C for 1000 h neither Al nor SiO_2 coatings protected type 316 stainless steel; however, oxidation undoubtedly propagated from uncoated edges. The Al coatings on several alloys exhibited evidence of extensive interdiffusion after the test at 1000°C, and, in one case, the coating oxidized severely. The Al coatings, however, generally protected the substrates against oxidation. The SiO_2 coatings, on the other hand, mostly detached from the substrates during tests in air and provided very little protection against oxidation.

The uncoated alloys had small specific weight changes of about 0.1 to 1.0 $ng/cm^2 \cdot s$ in air oxidation tests at 1000°C for 1000 h. At 1100°C for 1136 h, the weight changes for several alloys were in the range 0.4 to 3.5 $ng/cm^2 \cdot s$; however, Incoloy 800, Hastelloy N, and Haynes 25 exhibited much larger weight changes in the range 20 to 130 $ng/cm^2 \cdot s$. Alloys subjected to air oxidation at 1000 and 1100°C all had surface scales, subsurface porosity (or oxidation), and some exhibited intergranular attack. Considerable redistribution of Cr and other alloying elements occurred in the region near the oxidized surface with Cr being concentrated in the oxide scale.

Uncoated Inconel 625 exposed to an aluminum remelt furnace flue gases at 1000 to 1100°C exhibited extensive intergranular attack (more serious than occurred in air at the same temperatures), which proceeded at a projected rate of 2.8 mm/y in an exposure of 3230 h. Aluminum-coated Inconel 625 exposed in the same aluminum remelt furnace also corroded. In some areas the aluminum coating was fully protective, but only partially protective in other areas. In the latter areas intergranular attack

occurred at a projected rate of 1.2 mm/y (3230 h exposure). In all cases the aluminum coatings appeared to be degrading as indicated by oxidation or corrosion on the outer surface and by formation of pores or corrosion at the original coating-substrate interface. The results indicated that the coating gradually oxidizes and that corrosion of the substrate consists primarily of oxidation along grain boundaries, probably involving carbides or other grain-boundary precipitates containing Cr, Mo, and Nb. Aluminum-coated Inconel 601 exhibited similar intergranular attack to that observed in uncoated Inconel 625. The Al coating was missing from some regions on the Haynes 188 alloy. In those areas surface scale and intergranular attack occurred. In areas where the coating was intact the substrate was protected, although the coating was partially degraded. The SiO_2 coating was missing from the Inconel 625 specimen. As a result the specimen corroded in a typical manner with formation of scale and intergranular attack.

The SiC ceramics exposed to aluminum remelt furnace flue gases were covered with a glass slag. General corrosion was indicated at the slag-SiC interface which projected to about 0.5 mm/y (0.02 in./y) for several types of SiC ceramic. Mullite also exhibited a slag layer and corrosion at a rate of 0.2 mm/y (0.008 in./y). The alumina specimen had no significant corrosion. The only evidence of exposure was a 25-μm-thick surface layer, which was either a slag layer or a reaction layer.

CONCLUSIONS

The results that have been presented allow the following conclusions concerning the corrosion of materials in an aluminum remelt furnace environment.

1. Uncoated nickel-base alloys exhibited extensive corrosion characterized by scale formation and intergranular attack. A corrosion rate of 2.8 mm/y (0.11 in./y) for Inconel 625 probably represents a typical corrosion rate for several high-temperature alloys in the aluminum-furnace environment.

2. Aluminum-coated Inconel 625 corroded at a slower rate of 1.2 mm/y (0.05 in./y) than uncoated Inconel 625; therefore, aluminum coatings are potentially beneficial. Aluminum-coated alloys exhibited variable results, however, indicating that the coating process and/or coating-substrate combination are not yet optimized.

3. Metallic alloys are only marginally acceptable materials for critical components in FBWHR systems because of their propensity for corrosion. If metallic alloys are used, corrosion should be closely monitored because the intergranular attack observed in this work would probably cause significant weakening of the materials.

4. Ceramic materials had significantly lower corrosion rates than either uncoated or coated alloys. Based on corrosion behavior the SiC ceramics and oxide ceramics remain prime candidate materials for critical components of FBWHR systems.

ACKNOWLEDGMENTS

The authors wish to acknowledge the assistance of others at ORNL who participated in this work: J. R. Mayotte for optical measurement of specimens and photomicrographs; T. J. Henson for electron microprobe analyses; O. B. Cavin for X-ray diffraction analyses; L. Landau for spectrographic analyses; T. K. Roche and M. A. Janney for technical review of the draft; and F. W. Burns for preparation of the manuscript. We also thank Robert De Saro, Thermo Electron Corporation, who procured many of the materials, installed specimens in the aluminum remelt furnace, and subsequently recovered them for analysis.

REFERENCES

1. *High-Temperature Burner-Duct-Recuperator System Evaluation, Annual Report for October 1981–September 1982*, Babcock & Wilcox Company, BAW/LRC-5282, January 1984.

2. M. Coombs, D. Kotchick, and H. Strumpf, *High-Temperature Burner-Duct-Recuperator (HTBDR) Program: Annual Report, October 1981 through September 1982*, DOE/ID/12170, May 1983.

3. W. E. Cole, R. De Saro, and C. Joshi, *Fluidized-Bed Waste-Heat Recovery System Development, Semiannual Report, February 1–July 31, 1983*, DOE/ID/12302-4.

4. G. Y. Lai, M. F. Rothman, S. Baranow, and R. B. Herchenroeder, "Recuperator Alloys for High-Temperature Waste Heat Recovery," *J. Met.* **35**(7), 24–29, (July 1983).

5. K. V. Rao, M. F. Rothman, and R. B. Herchenroeder, "New Ni-Cr-Al-Fe-Y Alloy Promises Superior Oxidation Resistance in Service at Elevated Temperatures," *Ind. Heat.* **LI**(1), 35–38 (January 1984).

6. A. D. Russell, C. E. Smeltzer, and M. E. Ward, *Waste Heat Recuperation for Aluminum Furnaces*, GRI-81/0160, April 1983.

7. J. I. Federer and V. J. Tennery, *Corrosion of a Stainless Steel Waste Heat Recuperator*, ORNL/TM-7166, June 1980.

8. A. V. Seybolt, "Internal Oxidation in Heat-Resisting Stainless Steels Caused by Presence of Halides," *Oxid. Met.* **2**(2), 161–71 (1970).

9. M. K. Ferber and V. J. Tennery, *Evaluation of Tubular Ceramic Heat Exchanger Materials in Basic Coal Ash from Coal-Oil-Mixture Combustion*, ORNL/TM-8385, October 1982.

10. M. K. Ferber and V. J. Tennery, "Behavior of Tubular Ceramic Heat Exchanger Materials in Basic Coal Ash from Coal-Oil-Mixture Combustion," *Ceram. Bull.* **63**(7), 898–904 (July 1984).

11. J. I. Federer, T. N. Tiegs, D. M. Kotchick, and D. Petrak, *Analysis of Candidate Silicon Carbide Recuperator Materials Exposed to Industrial Furnace Environments*, ORNL/TM-9677, July 1985.

12. J. I. Federer and T. N. Tiegs, "Analysis of Candidate Silicon Carbide Recuperator Materials Exposed to Industrial Furnace Environments," to be published in *Advances in Science*, American Ceramic Society.

INTERNAL DISTRIBUTION

1–2. Central Research Library
3. Document Reference Section
4–5. Laboratory Records Department
6. Laboratory Records, ORNL RC
7. ORNL Patent Section
8. P. Angelini
9. P. F. Becher
10. R. A. Bradley
11. A. J. Caputo
12. R. S. Carlsmith
13. J. H. DeVan
14–18. J. I. Federer
19. H. W. Hoffman
20. H. S. Hsu
21. M. A. Janney
22. D. R. Johnson
23–27. P. J. Jones
28. R. R. Judkins
29. C. T. Liu
30. E. L. Long, Jr.
31. A. J. Moorhead
32. A. C. Schaffhauser
33. G. M. Slaughter
34–36. P. T. Thornton
37. R. J. Charles (Consultant)
38. G. Y. Chin (Consultant)
39. H. E. Cook (Consultant)
40. Alan Lawley (Consultant)
41. W. D. Nix (Consultant)
42. J. C. Williams (Consultant)

EXTERNAL DISTRIBUTION

43–44. AEROJET ENERGY CONVERSION COMPANY, P.O. Box 13222, Sacramento, CA 95813

L. Hoffman
H. W. Williams

45–46. AIRESEARCH MANUFACTURING COMPANY, 2525 W. 190th Street, Torrance, CA 90509

M. G. Coombs
D. M. Kotchick

47–48. BABCOCK AND WILCOX, P.O. Box 239, Lynchburg, VA 24505

D. Petrak
J. E. Snyder

49. C&H COMBUSTION, 1104 E. Big Beaver Road, Troy, MI 48083

R. G. Graham

50. CABOT CORPORATION, 1020 West Park Avenue, Kokomo, IN 46901

M. F. Rothman

51. COMBUSTION ENGINEERING, INC., 911 West Main Street, Chattanooga, TN 37402

C. H. Sump

52. CONSOLIDATED NATURAL GAS, 11001 Cedar Avenue, Cleveland, OH 44106

J. Bjerklie

53–55. COORS PORCELAIN COMPANY, 600 Ninth Street, Golden, CO 80401

C. Dobos
R. Kleiner
D. Roy

56. GAS RESEARCH INSTITUTE, 8600 West Bryn Mawr Avenue, Chicago, IL 60631

W. W. Liang

57–58. GTE PRODUCTS CORPORATION, Hawes Street, Towanda, PA 18848

J. L. Ferri
J. Gonzalez

59. HAGUE INTERNATIONAL, 3 Adams Street, South Portland, MA 04106

S. B. Young

60–61. IIT RESEARCH INSTITUTE, 10 West 35th Street, Chicago, IL 60616

J. W. Adams
D. C. Larsen

62–63. NORTON COMPANY, Worcester, MA 01606

B. D. Foster
M. L. Torti

64. PENNSYLVANIA STATE UNIVERSITY, 201 Steidle Building, University Park, PA 16802

R. E. Tressler

65–67. SOLAR TURBINES INCORPORATED, P.O. Box 85376, San Diego, CA 92138-5376

T. A. Argabright
C. E. Smeltzer
M. E. Ward

68. SOHIO ENGINEERED MATERIALS COMPANY, Structural Ceramics Division, P.O. Box 10549, Niagara Falls, NY 14302

J. Halstead

69–70. THERMO ELECTRON COMPORATION, P.O. Box 459, Waltham, MA 02254

W. E. Cole
R. DeSaro

71. UNIVERSITY OF ILLINOIS AT CHAMPAIGN-URBANA, 105 W. Goodwin Avenue, Urbana, IL 61801

M. K. Ferber

72. UNIVERSITY OF ILLINOIS AT CHICAGO, P.O. Box 4348, Chicago, IL 60680

M. J. McNallan

73–75. DOE, IDAHO OPERATIONS OFFICE, 550 2nd Street, Idaho Falls, ID 83401

F. Childs
J. B. Patton
W. H. Thielbar

76. DOE, OAK RIDGE OPERATIONS OFFICE, P.O. Box E, Oak Ridge, TN 37831

Office of Assistant Manager for Energy Research and Development

77–79. DOE, OFFICE OF INDUSTRIAL CONSERVATION, 1000 Independence Avenue, Forrestal Building, Washington, DC 20585

S. L. Richlen
J. R. Rossmeissl
W. B. Williams, Director

80–106. DOE, TECHNICAL INFORMATION CENTER, Office of Information Services, P.O. Box 62, Oak Ridge, TN 37831

For distribution by microfiche as shown in DOE/TIC-4500, Distribution Category UC-95 (Energy Conservation).